Chapter 2: Air pollution and dry deposition of nitrogen and sulphur in the AOSR estimated using passive samplers

Yu-Mei Hsu, Wood Buffalo Environmental Association, Fort McMurray, AB and Andrzej Bytnerowicz, US Department of Agriculture, Forest Service, Pacific Southwest Research Station, Riverside, CA, USA

2.1 Introduction

Ammonia (NH_3), nitrogen dioxide (NO_2) and nitric acid vapor (HNO_3) are important components of reactive atmospheric nitrogen (Nr) and major drivers of atmospheric nitrogen (N) dry deposition to forests and other ecosystems (Hanson and Lindberg, 1991; Lovett, 1994; Magnani *et al.*, 2007). Nitrogen dioxide is produced during oxidation of nitric oxide (NO) emitted during fossil fuel combustion, forest fires, and other natural and anthropogenic processes (Finlayson-Pitts and Pitts, 2000). Nitric acid is a final product of complex photochemical reactions between NO, NO_2, O^- and OH^- radicals (Seinfeld and Pandis, 2006). Ammonia emissions are caused by agricultural activities, biological decay processes, catalytic converters, smoldering phase of fires, and other activities (Krupa, 2003).

Sulphur dioxide (SO_2) may be released during natural processes (volcanic emissions, forest fires) and from anthropogenic activities such as combustion of fossil fuels, refining and smelting of sulphide ores, and other industrial processes (Legge *et al.*, 1998). Ambient ozone (O_3) is an important air pollutant which adversely affects human and forest health worldwide (Ainsworth *et al.*, 2012). It is produced during complex photochemical reactions between nitrogen oxides (NO_x), volatile organic compounds (VOCs) and carbon monoxide (CO), with reaction rates depending on ratios of the reactants and ambient conditions such as radiation and temperature of thermal inversions (Seinfeld and Pandis, 2006). All these pollutants are potentially phytotoxic at very high ambient concentrations, and their toxicity may be enhanced at low temperatures when rates of the biochemical detoxification mechanisms in plants are low (Bytnerowicz *et al.*, 1998).

Passive samplers for NH_3, NO_2, HNO_3, SO_2 and O_3 are useful for providing data describing ambient air conditions relevant to the health of forest plants. Passive samplers are simple to use, inexpensive, do not require electricity or air conditioned shelters and thus can be used in remote locations (Krupa and Legge, 2000; Bytnerowicz *et al.*, 2005). As such, passive samplers allow for spatial coverage of the areas of interest providing data that can be used for the generation of geostatistical maps of air pollutants distribution. The information gathered supports the better understanding of the atmospheric chemistry, attribution, deposition, regional trends, deposition,

regional imports and exports for those chemical species. The objectives of this chapter are (1) to characterize the spatial and temporal variations of NH_3, NO_2, HNO_3, SO_2 and O_3 concentrations in the Athabasca Oil Sands Region (AOSR); (2) to estimate the annual dry depositions of NH_3, NO_2, HNO_3 and SO_2; (3) to compare the dry deposition flux with IER (Chapter 3) and CALPUFF model (Chapter 4).

2.2 Methods

2.2.1 Monitoring, sampling and analysis for NH_3, HNO_3, SO_2, NO_2 and O_3

Passive samplers to collect NH_3, HNO_3, SO_2, NO_2 and O_3 were exposed to ambient air from towers above the tree canopy, where they were attached to cables on a pulley system, or on 2 m high posts in the industrial areas of the AOSR and in wetlands. The samplers were collected every month in the summer and every 2 months in winter.

Ambient concentrations of HNO_3 and NH_3 were monitored with passive samplers near the mining and industrial operations and in remote areas of the AOSR from 2005 until 2013. The monitoring network for NH_3 and HNO_3 consisted of 25 sites in 2005, gradually grew to 38 sites in 2009 and was reduced to 26 sites by 2010 - 2013. Passive samplers with two replicate filters coated with citric acid of the Ogawa design (Roadman *et al.*, 2003) were used for NH_3 monitoring. Ammonia reacts with citric acid on the filters producing ammonium citrate. After water extraction, ammonium (NH_4^+) concentrations in filter extracts were determined colorimetrically on a TRAACS 2000 Autoanalyzer, and ambient NH_3 concentrations were calculated based on a comparison of passive samplers against the collocated annular denuder systems (Koutrakis *et al.*, 1993). Three replicate HNO_3 samplers of the US Forest Service design (Bytnerowicz *et al.*, 2005) were used at each monitoring site. In these samplers, ambient air passes through a Teflon membrane and gaseous HNO_3 is absorbed on a Nylasorb nylon filter as nitrate (NO_3^-). Nylon filters from the samplers were extracted in nano-pure water, and NO_3^- concentrations in filter extracts were analyzed by ion chromatography (Dionex ICS 2000 LCD). Average ambient HNO_3 concentrations were calculated using calibration curves developed by comparing the passive samplers against the collocated annular denuder systems (Koutrakis *et al.*, 1993). In the field trials performed in Riverside, California, the samplers showed high accuracy (relative standard deviation of three replicate readings of ~5%). Exposed HNO_3 and NH_3 samplers were shipped to the USDA FS chemical laboratory in Riverside, California, where samplers' filters were extracted. The HNO_3 sampler extracts were analyzed for NO_3^- using ion exchange chromatography (Dionex ICS 2000 LCD), and the NH_3 sampler extracts for NH_4^+ were done colorimetrically with the TRAACS 2000 Autoanalyzer.

WBEA has operated a passive program for monitoring NO_2, SO_2 and O_3 at six sites (AH3, AH7, JP101, JP102, JP104 and JP107) since 2000. The all-season SO_2 passive sampling system (SPSS) (Tang *et. al*, 1997), the NO_2 passive sampling system (NPSS) (Tang *et al.*, 1999) and the O_3 passive sampling system (OPSS) (Tang and Lau, 2000) were used to estimate these parameters. After collection, SO_2, O_3 and NO_2 samples were extracted and analyzed by ion chromatography (DX-120, Dionex Corp., US) for SO_4^{2-}, NO_3^-, and NO_2^- concentrations by Maxxam Analytic Inc. (Hsu,

2013).

Air pollutant distribution maps based on the passive sampling results for NH_3, HNO_3, NO_2 and SO_2 were developed with inverse distance weighted (IDW) methods using the Geostatistical Analyst, an extension of the ESRI ArcGIS software. This method was selected because for the given data, characterized by relatively low number of samples, high spatial variation, and lack of trend or spatial pattern, it was providing the most accurate results (Johnstone *et al.*, 2001). Examples of distribution of NH_3, HNO_3, NO_2, reactive N and SO_2 were provided for winters (from November to April) 2010 and 2011 and summers (from May to October) 2011 and 2012. For O_3 concentration (Fig. 2.14) and deposition flux (NH_3-N, HNO_3-N, NO_2, total N and SO_2), kriging was used which provides an optimal interpolation estimate for a given coordinate location, as well as a variance estimate for the interpolation value.

2.2.2 Estimating dry deposition flux using the Multi-Layer Inferential Model

The National Oceanic and Atmospheric Administration (NOAA) multilayer inferential model (referred to as MLM) is used by the U.S. Environmental Protection Agency in the CASTNet monitoring program. CASTNet monitors ambient ozone (O_3), sulphur compounds (SO_2, and SO_4^{2-}), and nitrogen compounds (HNO_3, NO_3^-, and NH_4^+) throughout the United States (Clarke *et al.*, 1997). MLM is used to estimate dry deposition flux for these chemical species. A brief description of MLM and how it is used is provided below. More complete descriptions are offered by Meyers *et al.* (1998) and Cooter and Schwede (2000).

Chemical species dry deposition velocity (V_d) is estimated in MLM using an inference approach based upon an assumption that deposition flux can be estimated as the linear product of ambient concentration (C) and deposition velocity (V_d) (Meyers *et al.*, 1998; Wesely and Hicks, 2000):

$$\text{Flux} = C \times V_d \qquad \text{Equation 2.1}$$

Where C = chemical species concentration, and V_d = chemical species deposition velocity. The MLM is based on a resistance model framework analogous to Ohm's Law (Meyers *et al.*, 1998):

$$V_d = 1/(R_a+R_c) \qquad \text{Equation 2.2}$$

Where R_a = aerodynamic resistance between some height (a shallow sub-layer within the atmospheric constant flux layer, as a function of atmospheric turbulence and stability, and surface characteristics) above local ground and the canopy height, and R_c = total canopy resistance.

Deposition variations of the 2009-2012 annual average for NH_3 as N, HNO_3 as N, NO_2 as N, total N, and SO_2 as S were produced by using Surfer (Golden Software Inc.) for creating the spatial grids of data using Kriging (default options) from the point measurements and isopleths and ArcGIS for the maps.

2.3 Results and discussion

2.3.1 Ammonia (NH_3) ambient concentrations

Since the beginning of monitoring in May 2005, NH_3 concentrations were quite variable in time, without clear patterns, with peak values approaching 25 µg m^{-3} during the summer of 2011 (from May to October), though most of other values were generally <10 µg m^{-3} (Fig. 2.1). Ammonia was much higher in summers 2011 and 2012 than in winters (from November to April) 2010 and 2011 (Fig. 2.2) with the highest values in the centre and south western portion of the AOSR.

High NH_3 values in the S and SW portion of the monitored area in summer probably not related to oil processing. Most likely the high NH_3 values result from a dispersion were NH_3 emissions from the nearby agricultural lands north of Edmonton and a long-range transport of the pollutant from the Grand Prairie/Peace River farmland with prevailing westerly winds in summer (http://www1.agric.gov.ab.ca/$department/deptdocs.nsf/all/sag6452/$FILE/onl_s_19_twp_annual_normals_19712000.gif) into the AOSR. In dry summer conditions, NH_3 can be transported far away from the pollution-source areas as has been shown for the eastern parts of the Sierra Nevada affected by agricultural emissions from the Central Valley of California (Bytnerowicz *et al.*, 2014). This phenomenon was not observed in winter in absence of agricultural activities, and highest winter NH_3 values were limited to the industrial center of the AOSR. The highest values that occurred in summer 2011, about two- fold higher than in summer 2012, were most likely caused by extensive fires in northern Alberta during that period.

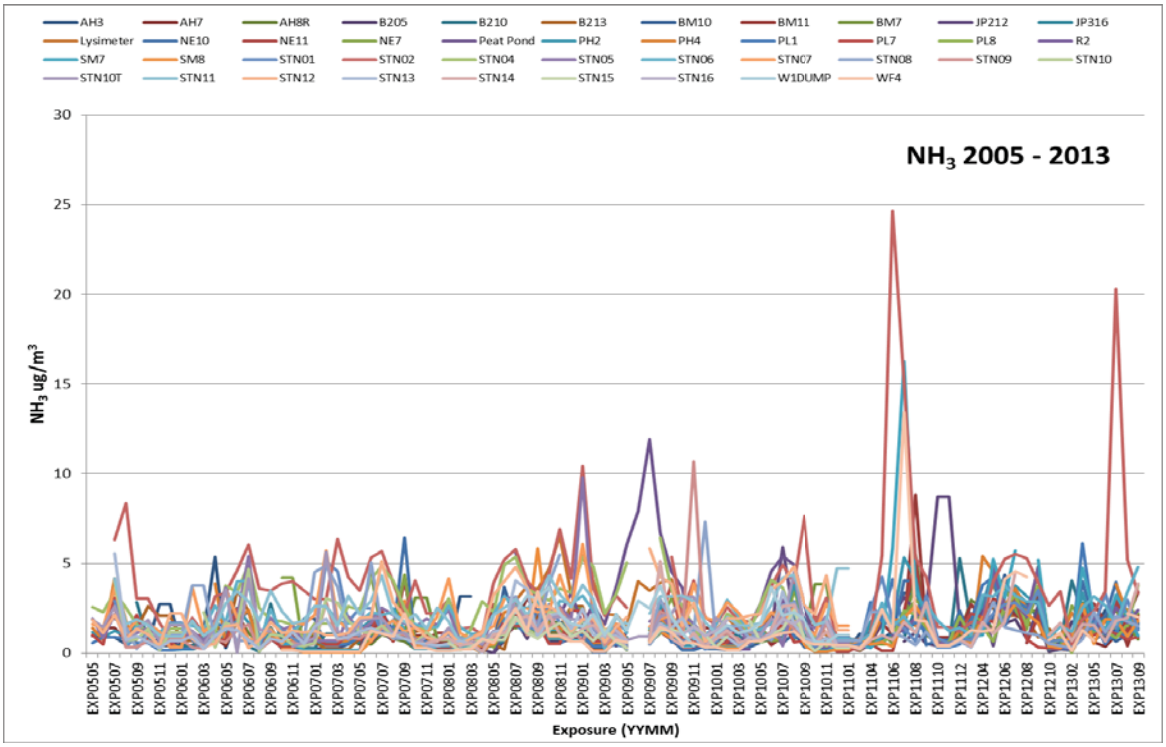

Figure 2. 1 Changes in NH_3 concentrations (µg m^{-3}) at all monitoring sites from May 2005 to September 2013.

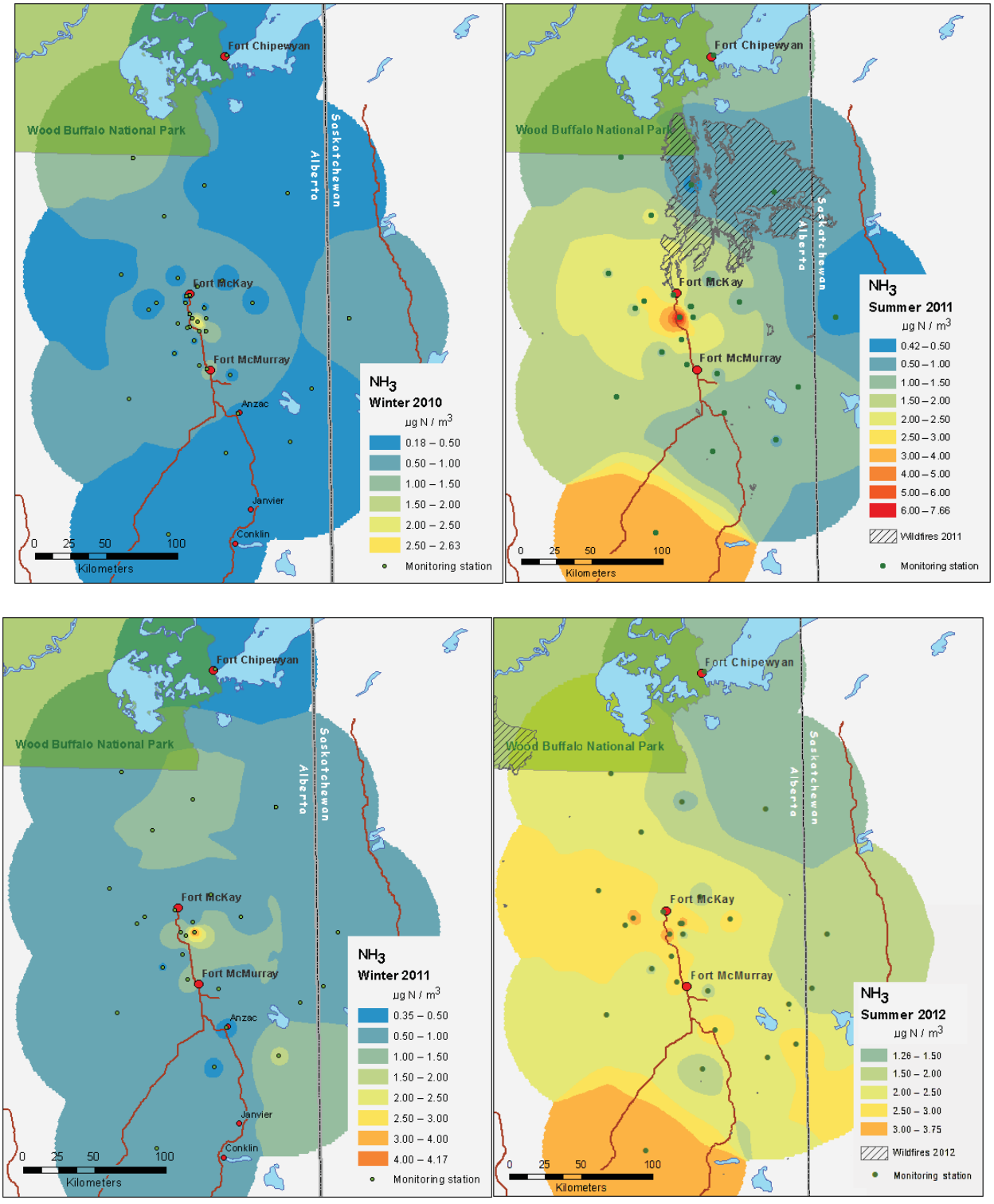

Figure 2. 2 NH_3 spatial variations in winter 2010, summer 2011, winter 2011 and summer 2012 (summer: from May to October; winter: from November to April) (Inverse Distance Weighted, IDW).

2.3.2 Nitric acid (HNO_3) ambient concentrations

From 2005 to 2013, HNO_3 concentrations were quite variable. Concentrations of this secondary pollutant were generally low in winter with no significant differences between the sites. In summer, HNO_3 concentrations were higher due to the photochemical nature of this pollutant. The highest values approaching 25 µg m^{-3} were measured during the 2011 summer season. The Richardson fire was an additional high source of HNO_3 in the NE, which contributed to the overall higher levels of HNO_3 experienced during the summer of 2011 shown during EXP1106 through EXP1109 (Fig. 2.3). In summer 2012 the highest HNO_3 concentrations occurred in the northern and south-western portions of the AOSR (Fig. 2.4). Long-range transport of HNO_3 produced during photochemical reactions in the urban-agricultural area of Edmonton could be responsible for elevated levels of the pollutant in SW portion of the AOSR. This phenomenon could resemble that seen in the San Bernardino Mountains of southern California affected by the Los Angeles photochemical air plume and the W slopes of the Sierra Nevada receiving polluted air masses from the Central Valley of California and the San Francisco Bay Area (Bytnerowicz *et al.*, 2014).

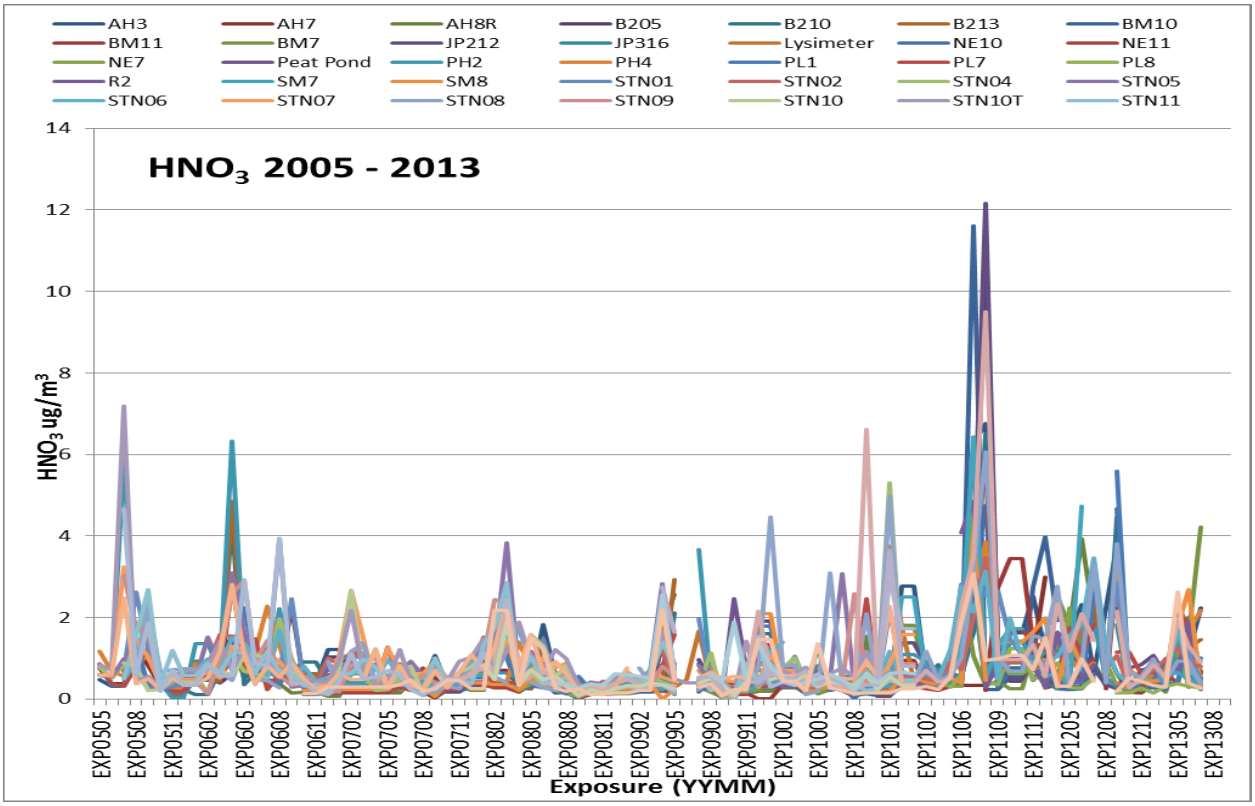

Figure 2. 3 Changes in HNO_3 concentrations (µg m^{-3}) in all monitoring sites from May 2005 until September 2013.

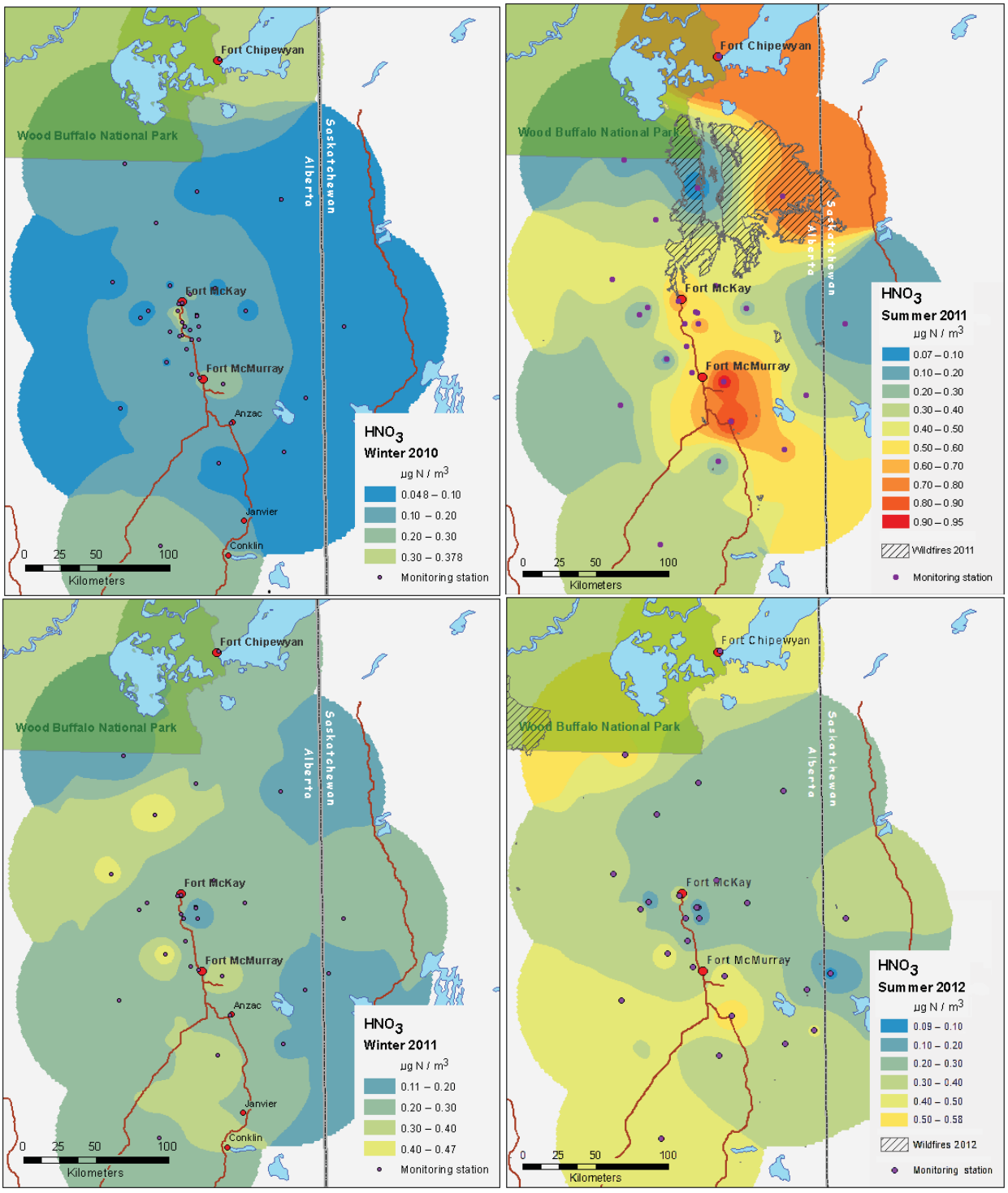

Figure 2. 4 HNO_3 spatial variations in winter 2010, summer 2011, winter 2011 and summer 2012 (summer: from May to October; winter: from November to April) (Inverse Distance Weighted, IDW).

2.3.3 Nitrogen dioxide (NO_2) ambient concentrations

The annual NO_2 concentrations from 2000 to 2013 (Fig.2.5) show that of the six sites sampled, NO_2 concentrations at JP102 and JP104 were higher than those at AH3, AH7, and JP101 and that concentration at JP104 varied significantly (Hsu, 2013). From 2000 to 2013, the highest NO_2 median concentrations occurred in 2009.

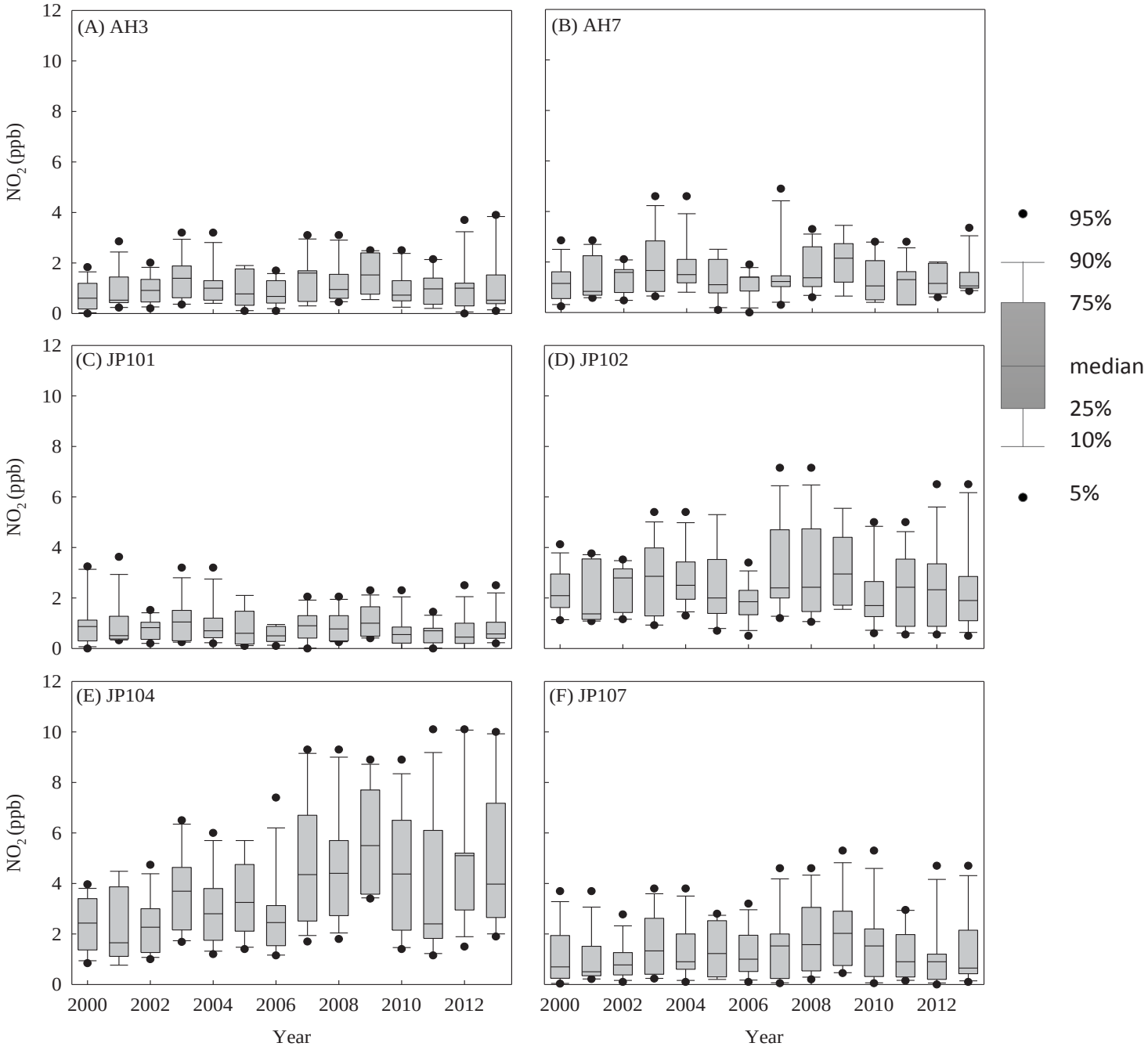

Figure 2. 5 Annual fluctuations in NO_2 concentrations at sites (A) AH3, (B) AH7, (C) JP101, (D) JP102, (E) JP104, and (F) JP107. From Hsu (2013).

The spatial variations of NO_2 concentration for winter 2010, summer 2011, winter 2011 and summer 2012 (Fig 2.6) show that the elevated NO_2 concentrations were observed near the major industrial emissions and residential areas for both summer and winter. The NO_2 concentrations in winter (2010 and 2011) were higher than those in summer (2011 and 2012). In the summer, the elevated NO_2 concentration is localized and limited to a small area close to the major emission sources. In the winter, the elevated NO_2 concentration is distributed more widely and to the north, due to the Athabasca Valley influence (prevailing wind direction). In winter months, meteorological condition (e.g., low temperature, stable atmosphere, less sunlight, low mixing height and ice surface) did not favor NO_2 dilution, NO_2 photochemical reaction, and NO_2 deposition in the atmosphere thus resulting in longer life time for NO_2.

Monthly NO_2 concentration variations from 2000 to 2013 (Fig 2.7) at the six sites show a strong seasonal variation: high in the winter and low in the summer months. The resulting higher NO_2 emissions in the winter included more NO_2 emitted to the atmosphere from both on-road and off-road vehicles at both idling and cold-start conditions and residential heating in the winter. At 57°N latitude, winter day length is very short (seven hours of daylight on Dec. 21st), and temperature is extremely low (average January high -13°C), and these factors necessarily result in slow photochemical reaction rates. Among the six sites, NO_2 concentrations were highest in the winter months at JP104 (median 7.2 ppb in December) and JP102 (median 4.2 ppb in December) as these sites are closer to two main emission sources with the NO_2 concentrations at AH3, AH7 and JP101 showing a similar pattern though with lower concentrations. However, JP107, 94 km north of oil sands operations, which is influenced by the Athabasca Valley orography, also had higher NO_2 concentrations during winter months. Comparing the annual average passive NO_2 concentrations from 2009 to 2012 with NO_2 predictions from CALPUFF model (Davies *et al.*, Chapter 4, Appendix 2.3) show that the NO_2 concentrations from the model were generally higher than those from the passive measurements, especially at JP102, JP212, AH7, NE11 and WF4 (Fig. 2.8) though the pattern of the spatial distribution between the two approaches was similar.

A non-parametric approach, the Sen-Thiel trend analysis of time series (Hsu, 2013), has been used on the 14-year monthly NO_2 data from AH3, AH7, JP101, JP102, JP104 and JP107. Table 2.1 lists the Sen slope (Sen) and the corresponding Sen-Theil 95% confidence interval (S_{low}, S_{high}). The results show the NO_2 concentrations at JP104 near the major emission sources to have increased during the past 14 years (Fig. 2.5) though AH3, AH7, JP101, JP102 and JP107 show no statistically significant differences.

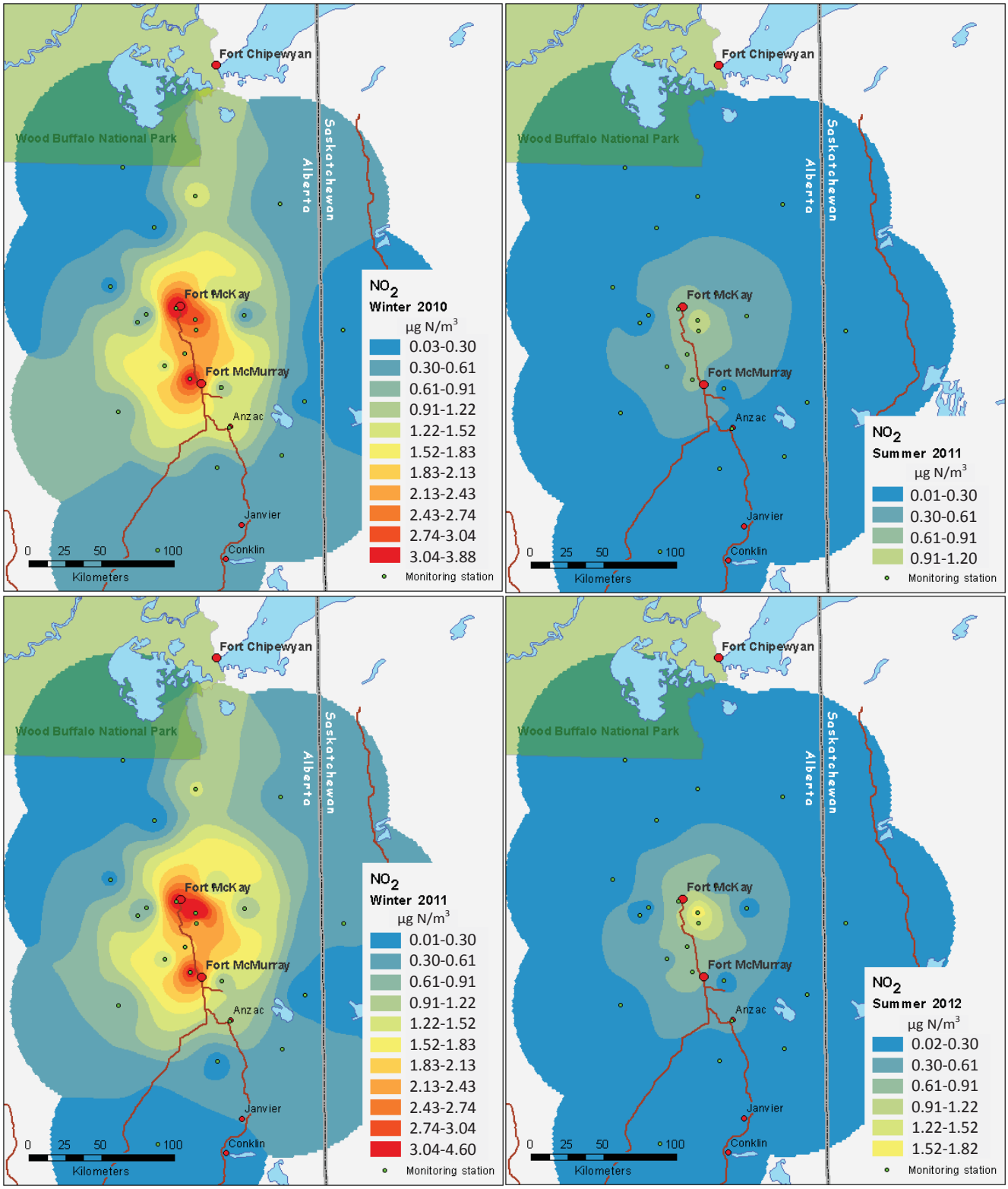

Figure 2. 6 NO_2 spatial variations in winter 2010, summer 2011, winter 2011 and summer 2012 (summer: from May to October; winter: from November to April) (Inverse Distance Weighted, IDW).

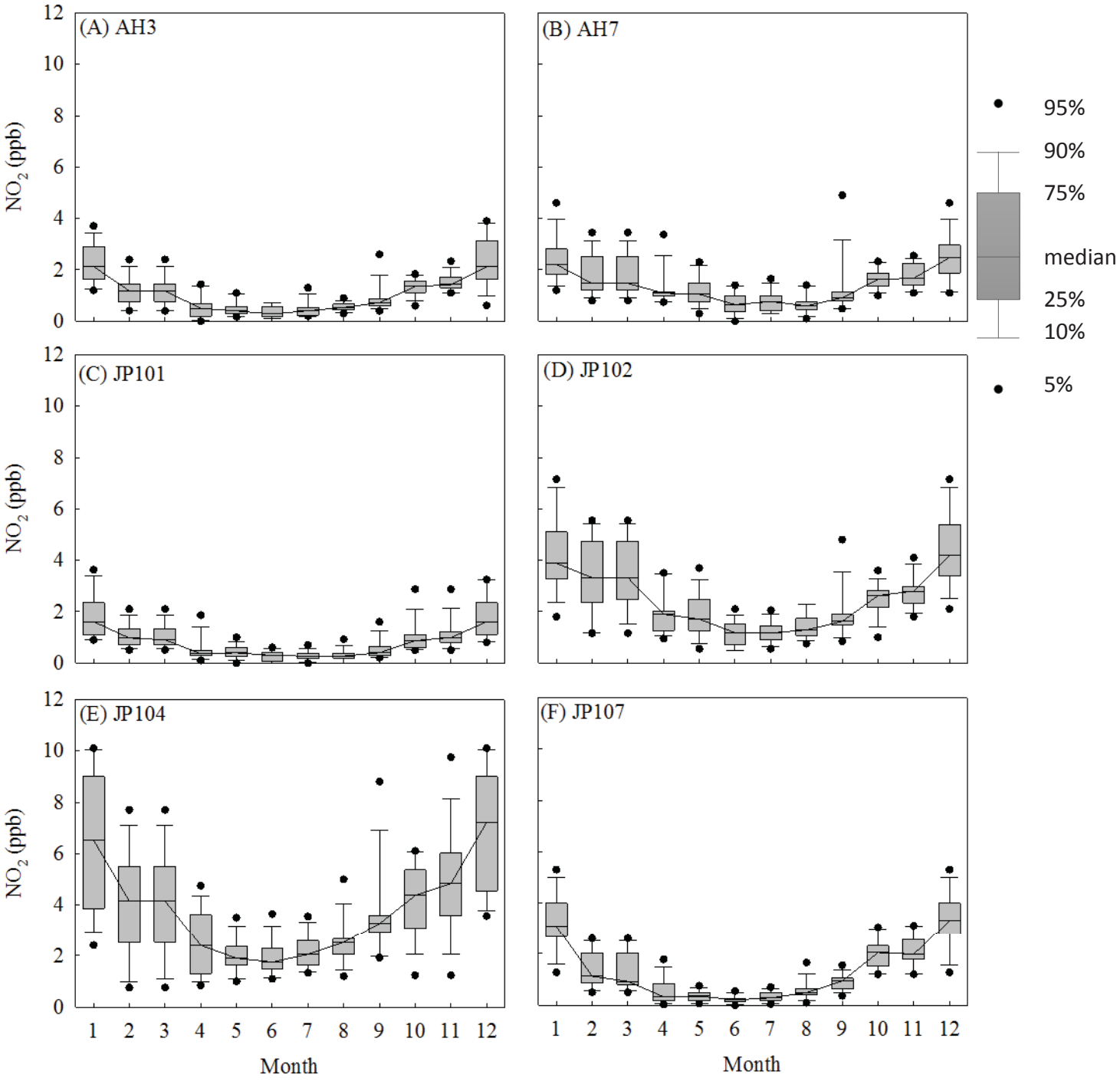

Figure 2. 7 Monthly variation in passively measured NO_2 concentrations from 2000 to 2013, (A) AH3, (B) AH7, (C) JP101, (D) JP102, (E) JP104, and (F) JP107. From Hsu (2013).

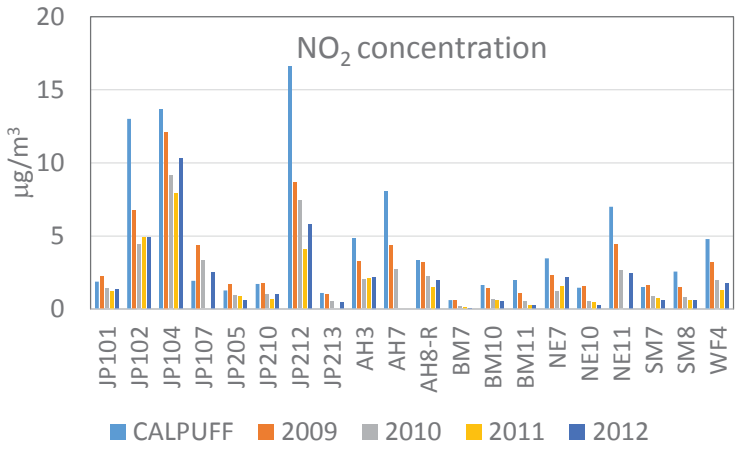

Figure 2. 8 Annual mean NO_2 concentrations from CALPUFF and passive samplers (2009 to 2012).

Table 2. 1 Sen-Theil test of slope significance for NO_2

	S_{low}	*Sen*	S_{high}	SLOPE*
AH3	–0.001286	0.000353	0.002562	No
AH7	–0.002273	0.000000	0.002404	No
JP101	–0.002740	–0.001087	0.000086	No
JP102	–0.004291	–0.000048	0.003704	No
JP104	0.009375	0.014778	0.021795	Yes
JP107	–0.001047	0.001187	0.004110	No

SLOPE*. No: no statistically significant slope (trend) at 95% confidence level.
Yes: statistically significant positive slope (trend) at 95% confidence level.

2.3.4 Total inorganic gaseous reactive N (N_r sum)

Combining the HNO_3, NH_3 and NO_2 concentration data on a network of 23 sites where all types of samplers were collocated, allowed calculation of inorganic gaseous reactive nitrogen (N_r sum) (Bytnerowicz *et al.*, 2010). Highest "N_r sum" levels were driven in winter by NO_2 concentrations and in summer mainly by NH_3 with a significant contribution of NO_2 and HNO_3. Geostatistical maps show that the areas in the vicinity of Fort McKay and Fort McMurray had the highest levels of N_r both in winter and summer. The highest N_r concentrations were observed in summer 2011 due to the wildfire emissions.

During that period the most affected regions were the central and southwestern portion of the AOSR. In summer 2012 highest levels of pollution were in the center as well as western and southern areas of the AOSR domain (Fig. 2.9, Appendix 2.4). These high levels of total reactive N in the S and SW portions of the AOSR could also be caused by a long-range transport of NH_3 and HNO_3 downwind of Edmonton and other urban and agricultural centers in central Alberta.

2.3.5 Sulphur dioxide ambient concentrations

Annual SO_2 concentrations from 2000 to 2013 at the six sampling sites are displayed Figure 2.10. SO_2 concentrations at JP102, AH7, and JP104 were higher than those from the other sites. The

spatial variations of SO_2 concentration for winter 2010, summer 2011, winter 2011 and summer 2012 are showed in Figure 2.10. The SO_2 spatial variations in summer 2011 and summer 2012 were similar and the elevated SO_2 concentrations were observed near the major industrial emissions, e.g., stacks. After being emitted from sources, SO_2 undergoes dilution, chemical reaction, dry deposition to surfaces, and the concentration decreases quickly.

The SO_2 distribution is localized and limited to a small area close to the major emitters in summer months. The SO_2 concentrations in winter were generally higher than those in summer. SO_2 spatial variations in winter 2010 and winter 2011 followed a similar pattern with the highest concentrations observed near the major emission sources. The lower mixing height and stable atmosphere, wind speed and wind direction are the major factors for the controlling SO_2 distribution in winter months. The annual average SO_2 concentrations from CALPUFF (Davies *et al.*, Chapter 4, Appendix 4.1) and passive samplers (Hsu, 2013) were very close at JP102, JP210, JP212, NE10 and SM8; the SO_2 concentrations from CALPUFF model were lower at few other sites (e.g., JP101, JP107, JP205, AH8-R) (Fig. 2.8). However, the SO_2 concentrations (Fig.2.10 and Fig.4.1) from two methods show the similar spatial pattern that the elevated SO_2 concentrations in the west of Fort McMurray and the east of Fort McKay were reported by both passive measurement and CALPUFF. Over the 14-year sampling period, the temporal trends of SO_2 concentration at the 6 sampling sites (Table 2.2), showed there was a decrease in air concentration at JP102 and JP104, perhaps a decrease at JP101 and that there was no statistically significant change at AH3, AH7 and JP107.

Table 2. 2 Sen-Theil test of slope significance for SO_2

	S_{low}	*Sen*	S_{high}	SLOPE*
AH3	-0.002353	-0.000725	0.000450	No
AH7	-0.004645	-0.001387	0.001389	No
JP101	-0.003571	-0.001613	0.000000	Perhaps decrease
JP102	-0.005712	-0.003305	-0.001042	Yes
JP104	-0.006111	-0.003724	-0.001756	Yes
JP107	-0.000727	0.000779	0.002273	No

* No: no statistically significant slope (trend) .Yes: statistically significant positive slope (trend) at 95% confidence level.

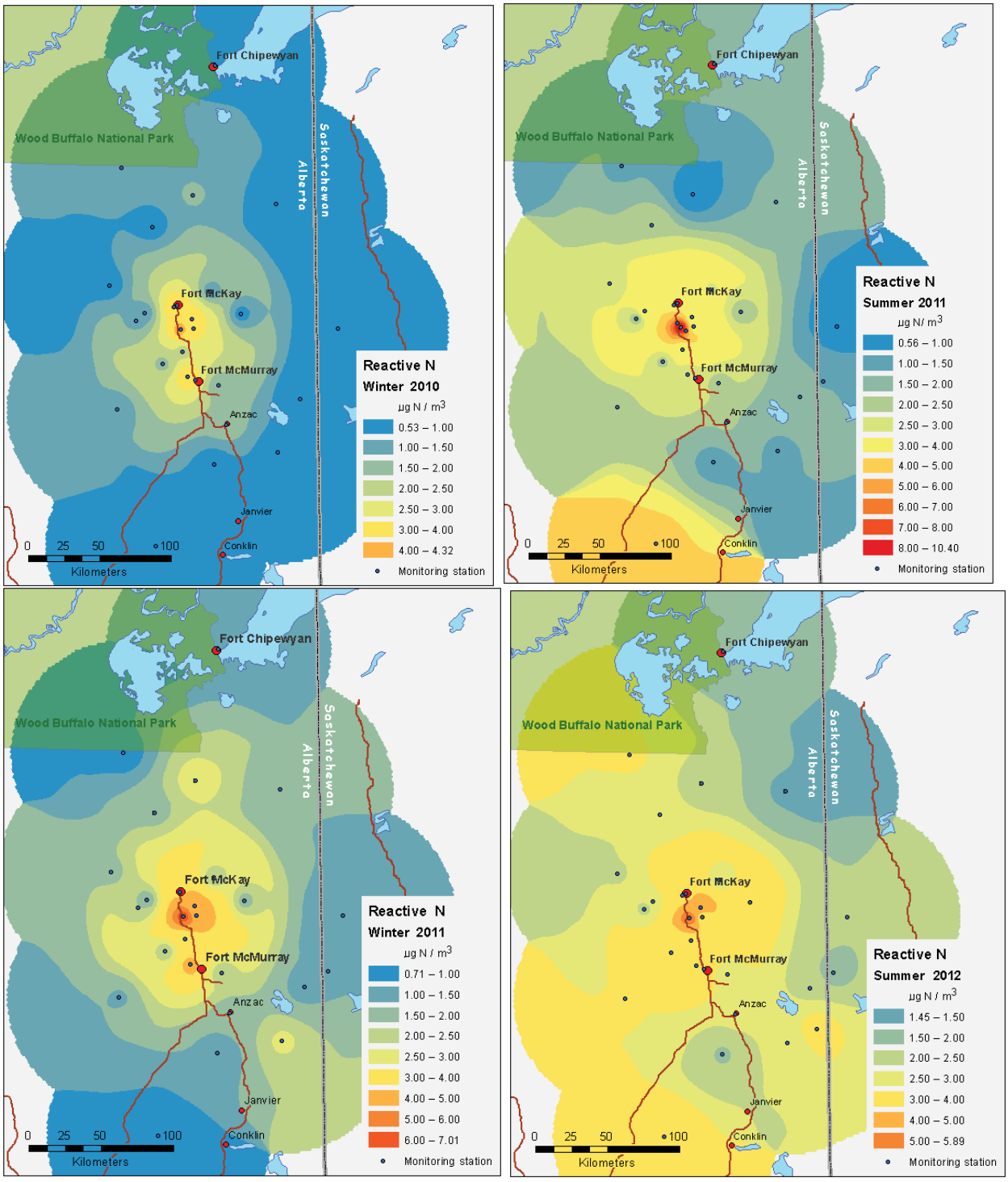

Figure 2. 9 Reactive gaseous inorganic N spatial variations in winter 2010, summer 2011, winter 2011 and summer 2012 (summer: from May to October; winter: from November to April) (Inverse Distance Weighted, IDW).

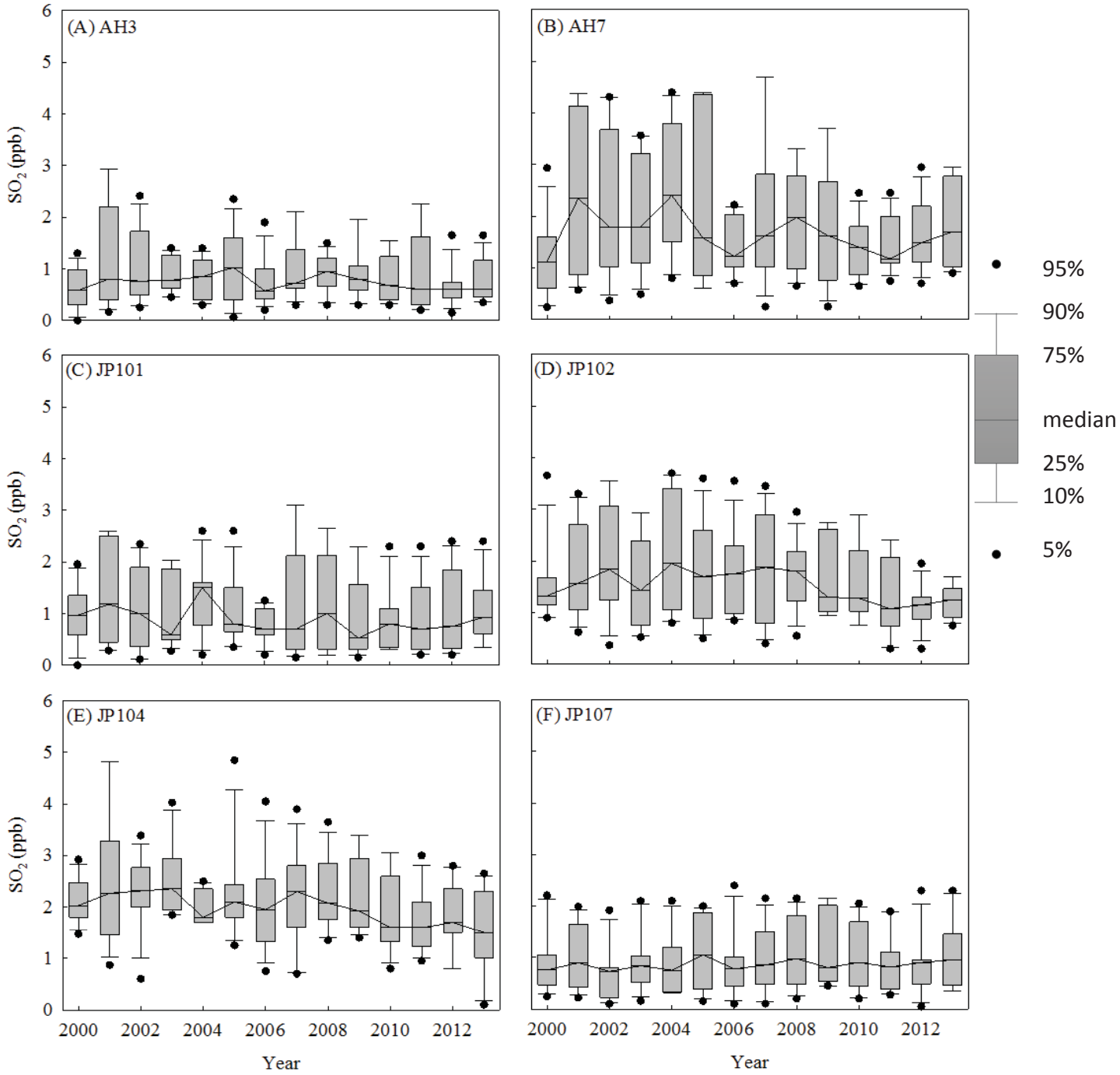

Figure 2. 10 Annual SO_2 air concentration value ranges at monitoring sites. From Hsu (2013).

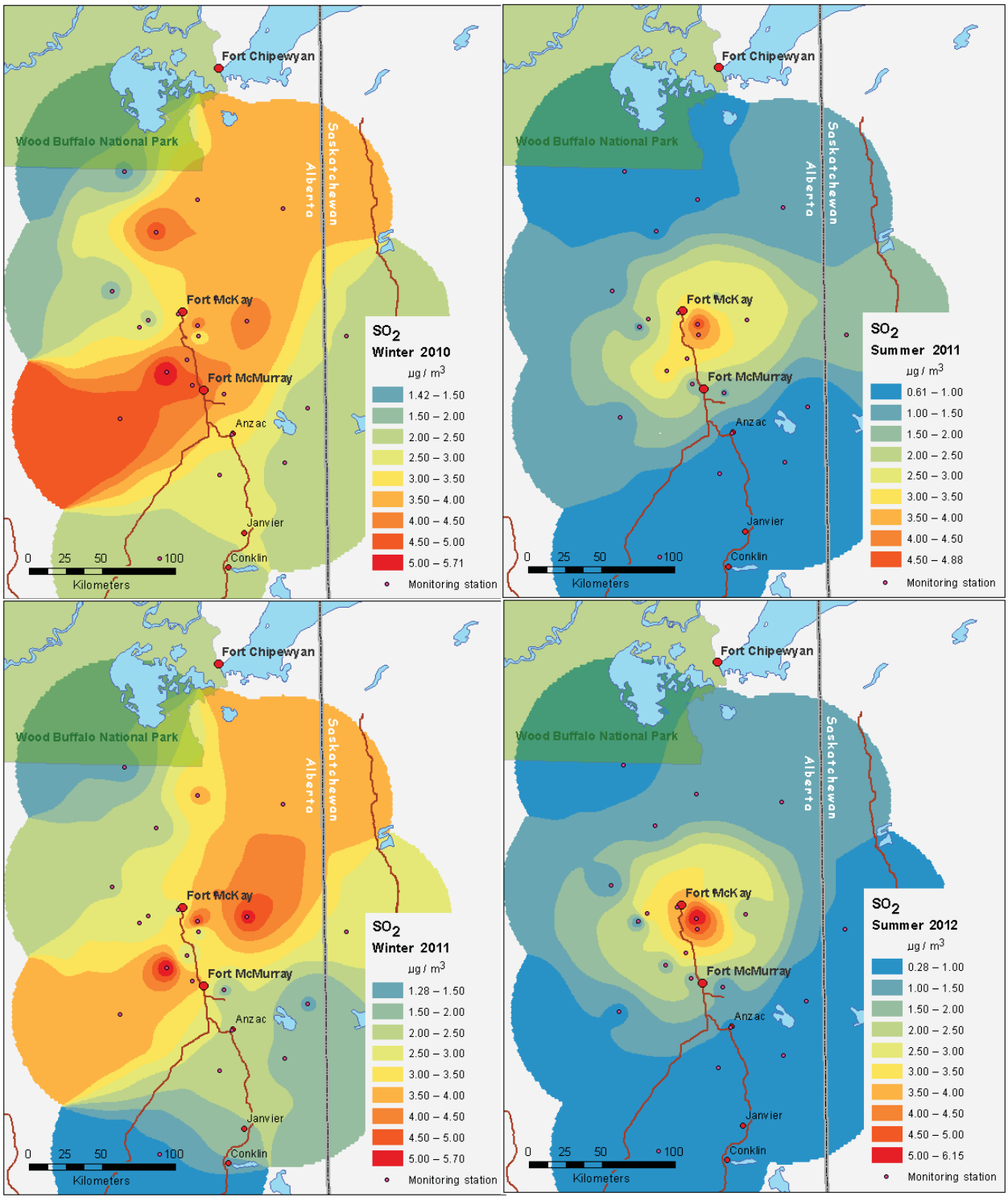

Figure 2. 11 SO_2 spatial variations in winter 2010, summer 2011, winter 2011 and summer 2012 (summer: from May to October; winter: from November to April) (Inverse Distance Weighted, IDW).

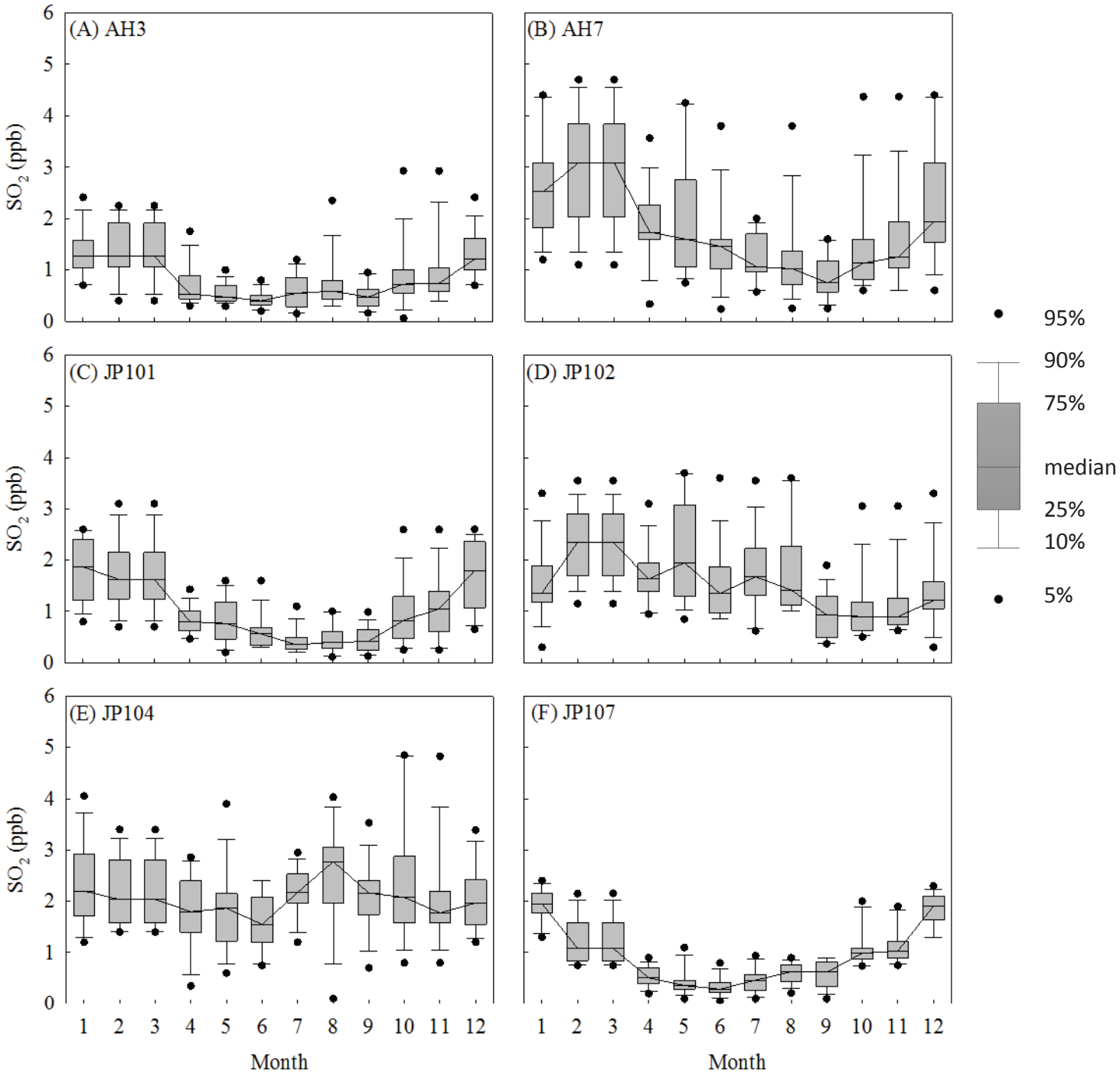

Figure 2. 12 Monthly variations in passively measured SO_2 concentrations from 2000 to 2013, (A) AH3, (B) AH7, (C) JP101, (D) JP102, (E) JP104, and (F) JP107. From Hsu (2013).

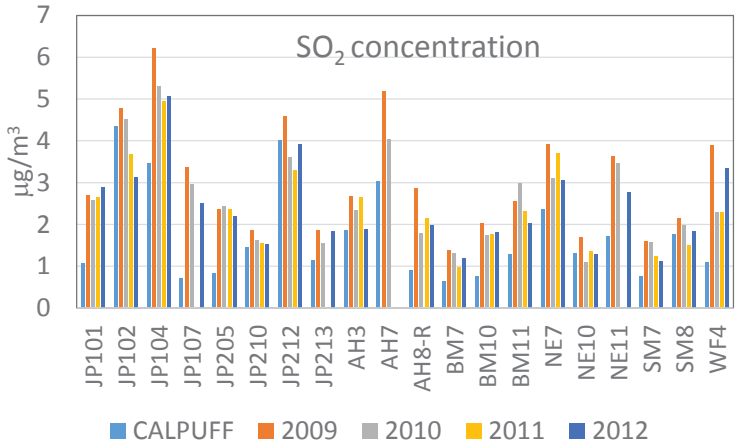

Figure 2. 13 Annual mean SO_2 concentrations from CALPUFF and passive samplers (2009 to 2012).

Three types of seasonal SO_2 concentration patterns were found using monthly SO_2 concentration variations from 2000 to 2013 (Fig. 2.12). No clear trend was observed at JP104. At sites AH3, JP101 and JP107, SO_2 concentrations had a seasonal pattern which was low in summer and high in winter. The lower mixing height, stable atmosphere and slow photochemical reactions are probably the major reasons for the relatively high SO_2 concentrations in the winter months (Hsu, 2013). In summer, SO_2 reactions including dry deposition and heterogeneous reactions with aerosols (Seinfeld and Pandis, 2006), are usually faster due to greater surface areas exposed to water, higher concentrations of oxidants and higher temperature. The distance (or time) between the emission sources and these three sampling sites (AH3, JP101 and JP107) allowed SO_2 to undergo direct deposition, heterogeneous reaction, and within plume dilution. AH7 and JP102, close to emission sources, showed similar patterns with the highest SO_2 median concentration occurring in February and March and the lowest observed September to November. It is possible that these two sites were sometimes directly impacted by emissions.

Table 2. 3 Sen-Theil test of slope significance for O_3

	S_{low}	*Sen*	S_{high}	SLOPE*
JP101	-0.041	-0.020	0.000	No
JP102	-0.042	-0.023	-0.005	Yes
JP104	-0.055	-0.035	-0.014	Yes
JP107	-0.035	-0.013	0.007	No
AH3	-0.036	-0.013	0.005	No
AH7	-0.044	-0.025	-0.003	Yes

SLOPE *, No: no statistically significant slope (trend) at 95% confidence level. Yes: statistically significant positive slope (trend) at 95% confidence level.

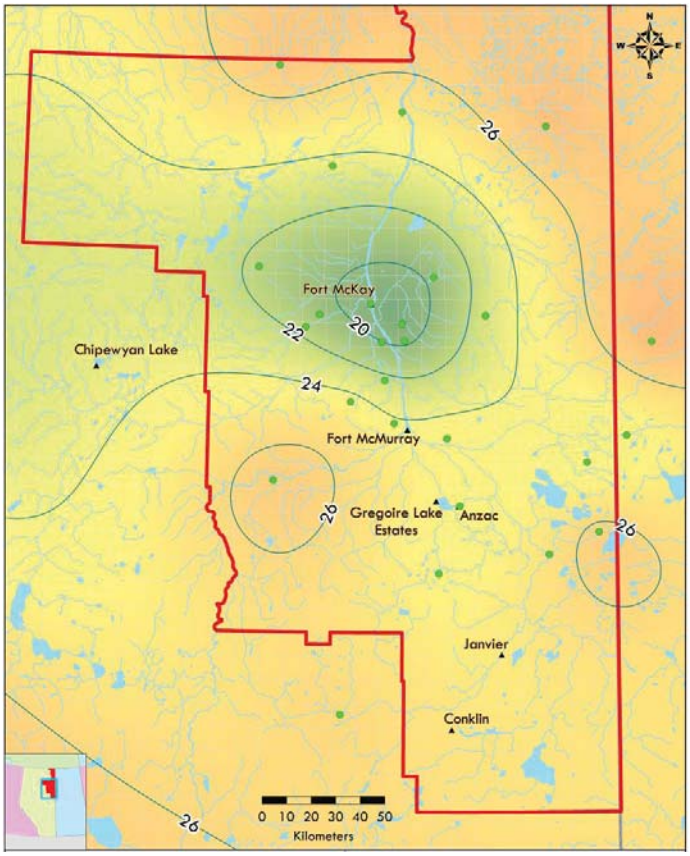

Figure 2. 14 2013 average O_3 concentration (ppb) in the AOSR (Kriging).

2.3.6 Ozone ambient concentrations

In 2013, the O_3 passive sampling program was conducted at 28 sites, including 23 remote sites (AH3, AH7, AH8-R, BM7, BM10, BM11, JP101, JP102, JP104, JP107, JP108, JP205, JP210, JP212, JP213, JP316, NE7, NE10, NE11, SM7, SM8, R2, and WF4) and 5 air monitoring stations (AMS 1, AMS 2, AMS 6, AMS 8 and AMS 14). The 2013 annual average O_3 concentration was low near the major NO_x emission sources, including stacks and mine fleets, and increased as the distance increased (Fig. 2.14). The lowest 2013 annual average concentration was 16.0 ppb at R2 south of Fort McKay and the highest concentration was 28.7 ppb at JP316 and AMS 8 (Fort Chipewyan). The low O_3 concentration in the industrial area was likely due to O_3 titration. Nitric oxide emitted from sources (stack and mine fleets) reacts with available ambient O_3 to form NO_2 and O_2. The O_3 spatial variation suggests titration effect (low O_3 concentration) is limited to the area close to industrial activity.

The passive dataset comprises a monthly O_3 time series covering the time period from January 2000 to December 2013 (Table 2.3) and Sen-Thiel trend analyses were done for the 14 year data set from AH3, AH7, JP101, JP102, JP104 and JP107. The data show that the O_3 concentrations from 2000 to 2013 have decreased at JP102, JP104 and AH7, sites which are all close to major oil sands activities. As indicated in section 2.3.3, the NO_2 concentration at JP104 has increased from 2000 to 2013 so that O_3 titration could be the reason to explain the decrease in O_3 concentration and the increase in NO_2 concentration at JP104. No statistically significant temporal changes in O_3 concentration were detected for three sites, JP101, JP107 and AH3 (Hsu, 2013).

2.3.7 Nitrogen and sulphur deposition estimates based on passive sampler data

Monthly Deposition Velocities (V_d) for NH_3, HNO_3, NO_2 and SO_2 from 2000 to 2012 at AMS 1 are generally higher in summer than in winter (Fig. 2.15). The maximum V_d occurred in July for both NH_3 and NO_2, in summer months (May, June and July) for HNO_3, and in March and July for SO_2. Since V_d for NH_3, HNO_3, NO_2 and SO_2 is influenced by both ground surface and aerodynamic resistance, higher V_d reflects the more foliated and water ground cover (compared to snow and dust) with the combination of higher wind speeds in spring. Hence, the V_d is generally higher in summer months. Estimated V_d values of these species are within a reasonable range compared

to earlier studies (Brook *et al.*, 1999; Krupa, 2003; Schwede *et al.*, 2011; Sickles and Shadwick, 2007a; Sickles and Shadwick, 2007b; Zhang *et al.*, 2009). In North America, two models (MLM and Big Leaf Model) are used for long-term monitoring network (including CASTNet and CAPMoN) to calculate the V_d and dry deposition. Schewede *et al.* (2011) have compared these two models and concluded the V_d of SO_2 from MLM was lower than that from BLM but it is unclear how accurate the models are or which is the best for the AOSR. The MLM approach was used, taking this uncertainty in to account. Further calculations using BLM are recommended to determine which model might be more suitable for the AOSR.

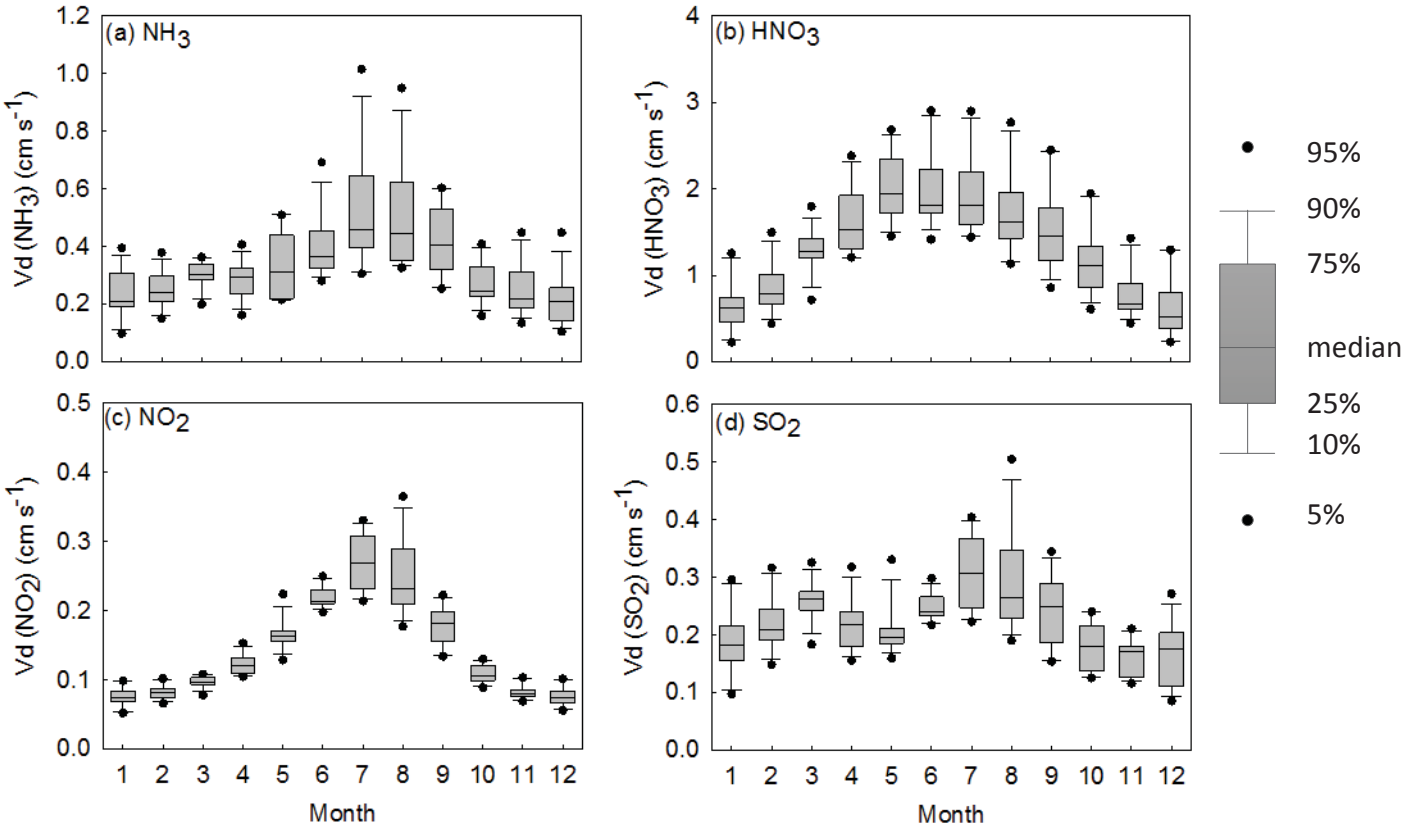

Figure 2. 15 Monthly deposition velocities of (a) NH_3, (b) HNO_3, (c) NO_2 and (d) SO_2 at AMS 1 (from 2000 to 2012) calculated by MLM.

2.3.7.1 Ammonia dry deposition

Ammonia deposition values for 23 monitoring sites were calculated for individual years during 2006 – 2012 period and showed values ranging from 0.38 kg N ha^{-1} yr^{-1} at JP205 to 2.35 kg N ha^{-1} yr^{-1} at SM7 in 2011 (Appendix 2.1). A map of average distribution for the 2009 – 2012 period (Fig. 2.16, left) shows two areas of high NH_3 deposition – one in the center of the AOSR between Fort McMurray and Fort McKay; and the second larger area in the southern portion of the monitoring area. While the first area can reflect deposition caused by elevated NH_3 emissions and concentrations during oil sands operations at the AOSR, the second most likely is caused by dispersion of NH_3 emissions from the agricultural lands north of Edmonton and a long-range transport of the pollutant from the Grand Prairie/Peace River farmlands with the prevailing

westerly winds in summer. (http://www1.agric.gov.ab.ca/$department/ deptdocs. nsf / all / s ag6452/$FILE/onl_s_19_twp_annual_normals_19712000.gif). In general, the determined 4-year average NH_3 deposition ranged between 0.7 to 1.25 kg N ha^{-1} yr^{-1}. These values were higher than the dry deposition values for HNO_3 or NO_2.

Passive samplers were collocated with IER samples (Fenn, Chapter 3) at nine sites including AMS 1, AMS 14, JP101, JP102, JP104, JP107, JP210, JP212 and JP213 from the summer in 2008. The NH_4^+ dry deposition from passive data with MLM and the NH_4^+ deposition from IER open/throughfall samples (wet and dry) were similar (Fig. 2.17). All results show that the NH_4^+ deposition in summer was higher than that in winter.

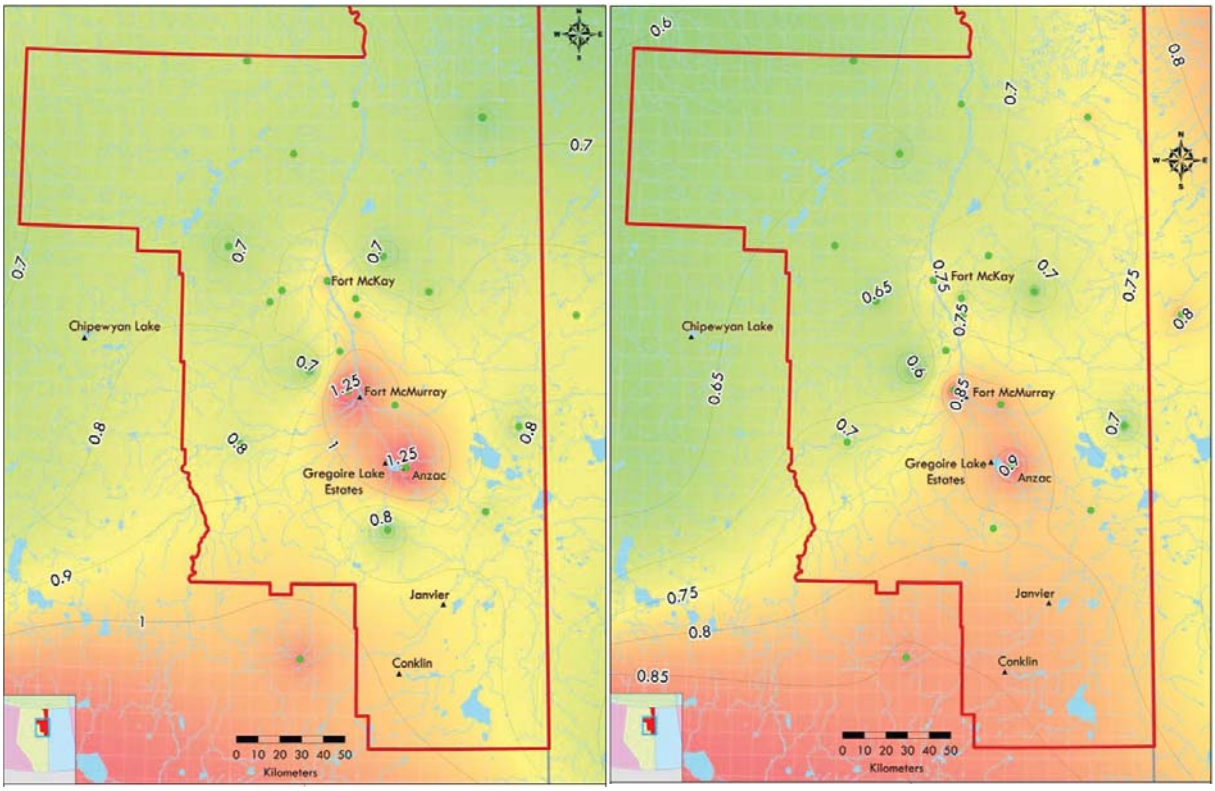

Figure 2. 16 NH_3-N (left) and HNO_3-N (right) deposition average from 2009 to 2012 in the AOSR in kg N ha^{-1} yr^{-1} (Kriging).

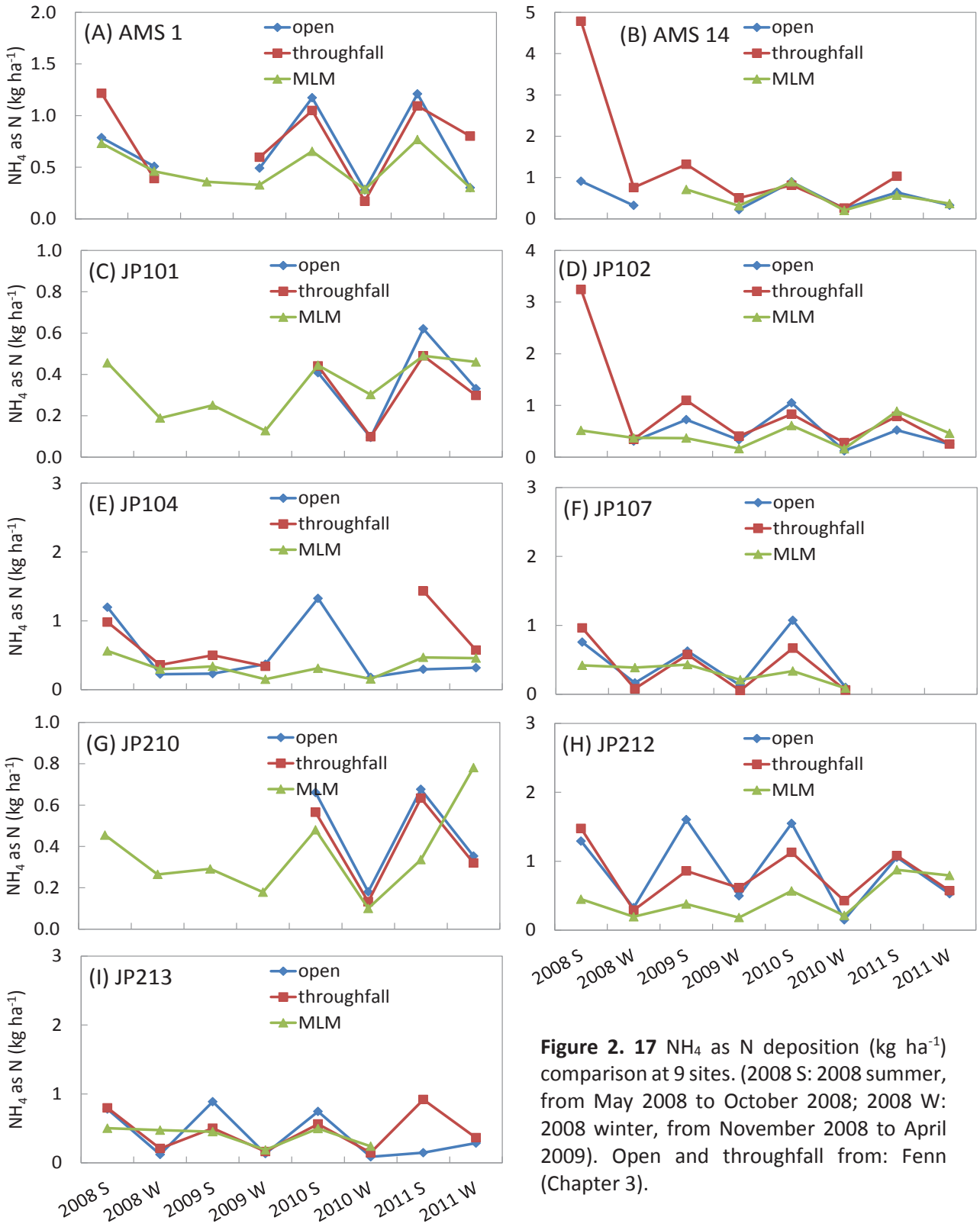

Figure 2. 17 NH_4 as N deposition (kg ha^{-1}) comparison at 9 sites. (2008 S: 2008 summer, from May 2008 to October 2008; 2008 W: 2008 winter, from November 2008 to April 2009). Open and throughfall from: Fenn (Chapter 3).

2.3.7.2 HNO_3 dry deposition

Deposition of HNO_3 during the 2006 – 2012 period ranged between 0.16 kg ha^{-1} yr^{-1} at AH8 in 2007 and NE11 in 2009 to 2.70 kg ha^{-1} yr^{-1} at BM7 in 2012 (Appendix 2.2). Similarly to NH_3, the highest HNO_3 deposition values were determined in the central area of the AOSR and in its southern portion (Fig. 2.16, right). The deposition distribution pattern was similar to that of the HNO_3 summer concentrations (Fig. 2.4). The 4-year average deposition values for this pollutant ranged between 0.3 and 0.9 kg N ha^{-1} yr^{-1}, and were slightly lower than the NH_3 deposition values (Fig. 2.17). These values were in the similar range as those for NO_2 deposition (Fig. 2.18, left).

2.3.7.3 NO_2 deposition

NO_2 deposition is a component of total N deposition for the AOSR. Nitrogen dioxide dry deposition was estimated at 23 sites from 2009 to 2012 (Appendix 2.3) with an annual average NO_2 -N deposition ranging from 0.03 kg $ha^{-1}yr^{-1}$ in BM7 to 0.98 kg $ha^{-1}yr^{-1}$ at AMS 6 (Fig. 2.18,(left)). After NO_x emitting from the sources, NO_x undergoes dilution and photochemical reactions. The major NO_2 removal mechanism from the atmosphere is a photochemical reaction, reacting with OH radicals during the daytime and NO_3 radicals at night. The life time of NO_2 is around one day (Seinfeld and Pandis, 2006) during the summer condition in the AOSR and with the short life time, the major NO_2 deposition is localized.

The greatest NO_2 deposition (Fig. 2.18, (left)) occurred in places where major oil sand operation activities took place and where communities existed. It is likely that elevated NO_2 deposition resulted from industrial emissions (e.g., stacks and mine fleet) at JP104 and from local community activities (e.g., personal vehicles, transport trucks) at AMS 6. The dry deposition results from the passive NO_2 and HNO_3 data with MLM calculation at nine sites including AMS 1, AMS 14, JP101, JP102, JP104, JP107, JP210, JP212 and JP213 are in the range of IER bulk (open) and throughfall results (Fig. 2.19).

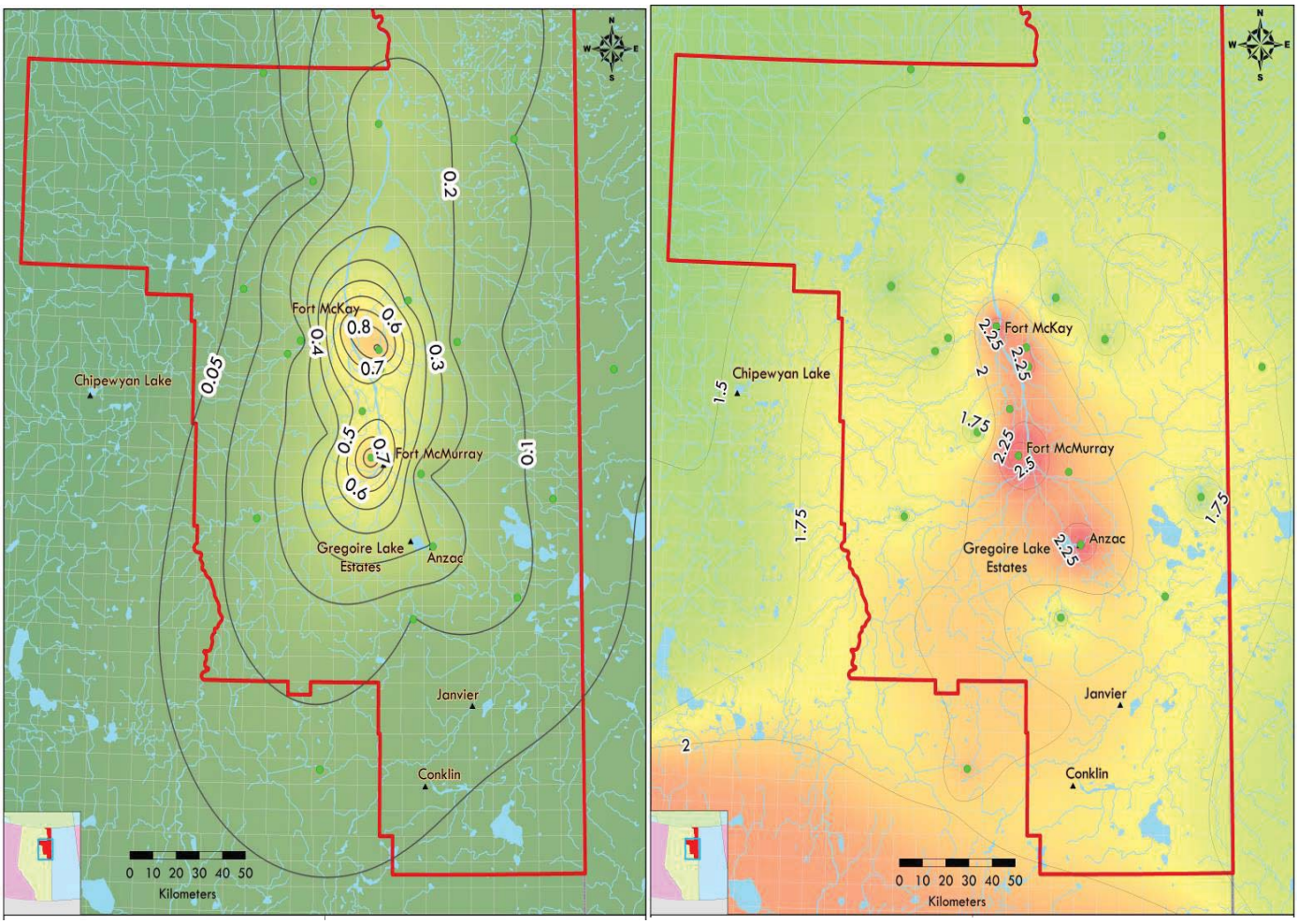

Figure 2. 18 NO_2-N (left) and total N (right) deposition average from 2009 to 2012 in the AOSR in kg N ha^{-1} yr^{-1} (Kriging).

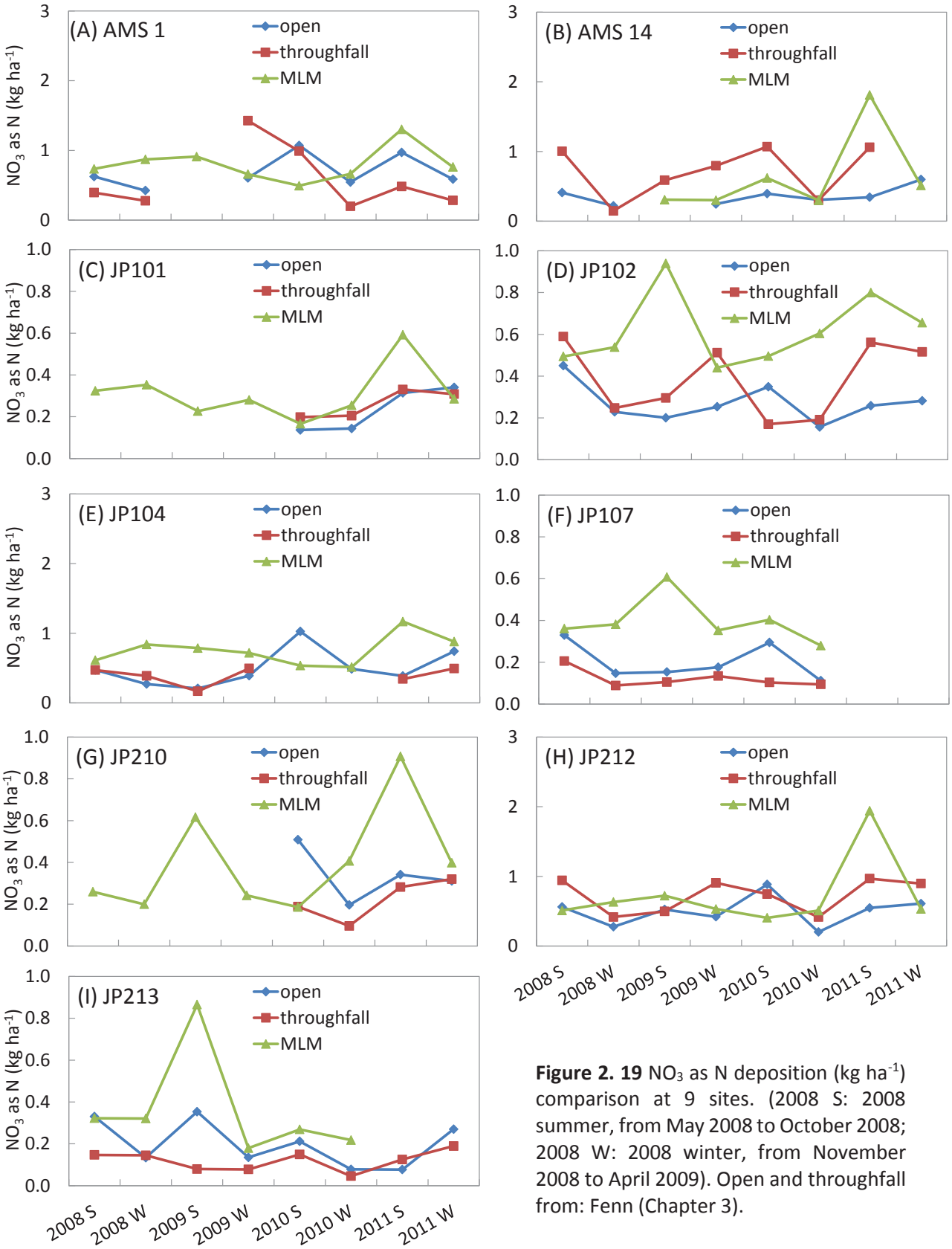

Figure 2. 19 NO_3 as N deposition (kg ha^{-1}) comparison at 9 sites. (2008 S: 2008 summer, from May 2008 to October 2008; 2008 W: 2008 winter, from November 2008 to April 2009). Open and throughfall from: Fenn (Chapter 3).

2.3.7.4 Total reactive N deposition

Total deposition of reactive inorganic gaseous N during the 2006 – 2012 period ranged between 0.78 kg N ha^{-1} yr^{-1} at AH8 in 2007 to 4.97 kg N ha^{-1} yr^{-1} at AMS14 in 2012 (Appendix 2.4). A map of the average N distribution for the 2009 – 2012 period (Fig. 2.18, (right)) shows two areas of high N deposition – one in the center of the AOSR between Fort McMurray and Fort McKay with values reaching 2.5 kg N ha^{-1} yr^{-1}, and the second in the southern portion of the monitoring area with values approaching 2 kg N ha^{-1} yr^{-1}. Distribution patterns for total deposition of inorganic gaseous N are similar to those of the NH_3 deposition indicating relative importance of that pollutant. Nitric acid had a strong contribution to elevated N deposition in the southern AOSR, while NO_2 contributed mainly to the elevated levels between Fort Mc Murray and Fort McKay.

While higher deposition in the center of the AOSR is mainly related to the industrial emissions of NO_2 and NH_3, while the elevated deposition values in the southern part of the AOSR could be caused by agricultural activities in central and western Alberta and long-range transport of NH_3 (see the above discussion for NH_3 and HNO_3). It can be shown that nitrogen deposition from inorganic reactive gaseous pollutants is an important component of total (wet and dry) N deposition. While values of total wet and dry deposition calculated with the modeled CALPUFF are usually higher, the CALPUFF results were surprisingly lower at a few sites (BM10, BM7, and SM7). There is a need to examine performances of the multilayer and CALPUFF models.

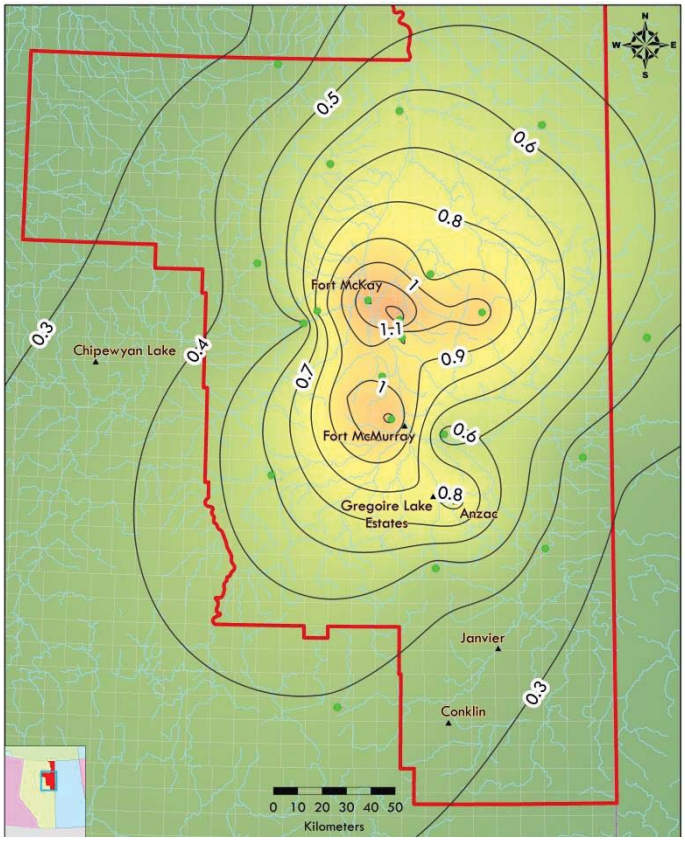

Figure 2. 20 2009-2012 SO_2 (as S) annual average deposition (kg ha^{-1} yr^{-1}) in the AOSR (Kriging).

2.3.7.5 Sulphur dioxide deposition

Sulphur dioxide (SO_2) in the ambient air is removed by dry and wet deposition and oxidized to sulphate. The SO_2 residence times are 60, 100 and 80 hours for removing by dry deposition, wet deposition and chemical reaction, respectively, and the overall residence time is 25 hours when three mechanisms are combined (Seinfeld and Pandis, 2006). All three removal mechanisms are important for ambient SO_2 concentration. The SO_2 as S dry deposition was calculated at 13 sites from 2006 to 2008 and 23 sites from 2009 to 2012. Annual averages ranged from 0.26 kg ha^{-1} yr^{-1} in BM7 in 2011 to 2.04 kg ha^{-1} yr^{-1} at AMS 1 in 2006. From 2006 to 2008, AMS 1 had the highest SO_2-S deposition with values of 2.04, 1.91 and 1.61 kg ha^{-1} yr^{-1} in 2006, 2007 and 2008, respectively. From 2009 to 2012, JP104 had the higher SO_2 deposition than

AMS 1 (Fig. 2.20). The lowest SO_2 as S deposition was 0.32 kg $ha^{-1}yr^{-1}$ in BM7, 80 km north of Fort McKay. JP104, AMS 1, AMS 6, and NE7 had higher SO_2 deposition rate, 1.24, 1.19, 1.12 and 1.05 kg ha^{-1} yr^{-1}, respectively.

The elevated SO_2 deposition was observed near the major SO_2 emission sources, i.e., stacks (Fig. 2.20). Based on Environment Canada's National Pollution Release Inventory (NPRI), there were two major SO_2 emission sources (stacks) in the oil sand operation area and the highest deposition occurred in the same area. SO_2 deposition trended towards the east and south most likely due to the Athabasca Valley influence. The increased SO_2 deposition was also reported in Fort McMurray, an urban transportation hub.

The SO_2 dry deposition estimated using passive SO_2 concentration with MLM was compared to the sulphate deposition from IER (Chapter 3) as shown in figure 2.21 and CALPUFF model (Chapter 4) and the MLM estimate was considerably lower than the bulk/throughfall and CALPUFF model values. MLM and Big-Leaf Model (BLM) are used by USEPA and Environmental Canada for dry deposition estimates of SO_2, NH_3, NO_2, and HNO_3. Schewede *et al.* (2011) conducted an intercomparison of MLM and BLM and concluded that the V_d of SO_2 from MLM and BLM were uncorrelated and the median V_d of SO_2 from MLM was 49% lower than that from BLM. Sickles and Shadwick (2007) estimated the S and N deposition in the eastern U.S. and also identified that the Vd of SO_2 might be underestimated for forested canopies. The MLM deposition was compared with CALPUFF deposition to understand if the MLM could be a reliable tool for deposition calculation in the AOSR although the CALPUFF deposition consists of both dry and wet depositions. It is expected that the deposition from both MLM and CALPUFF had similar patterns and the dry deposition should be 20%-60% of total deposition. Both MLM and CALPUFF conclude that the elevated SO_2 deposition was identified in the west of Fort McMurray, the east of Fort McKay and Anzac (Fig. 2.20 and Fig. 4.2). IER bulk (open) sampler mainly collects wet deposition and throughfall sample includes wet deposition and dry deposition, at least partially, as integrated by the natural surface area of the forest canopy. Assuming the difference of SO_4 as S deposition from IER bulk (open) and throughfall sample is SO_4 as S dry deposition. The SO_2 as S dry deposition from MLM is still lower than that from IER. It is possible that the MLM underestimated the SO_2 as S dry deposition for near source calculation. Further investigation should be conducted to improve the model calculation or to apply the BLM for S deposition calculation.

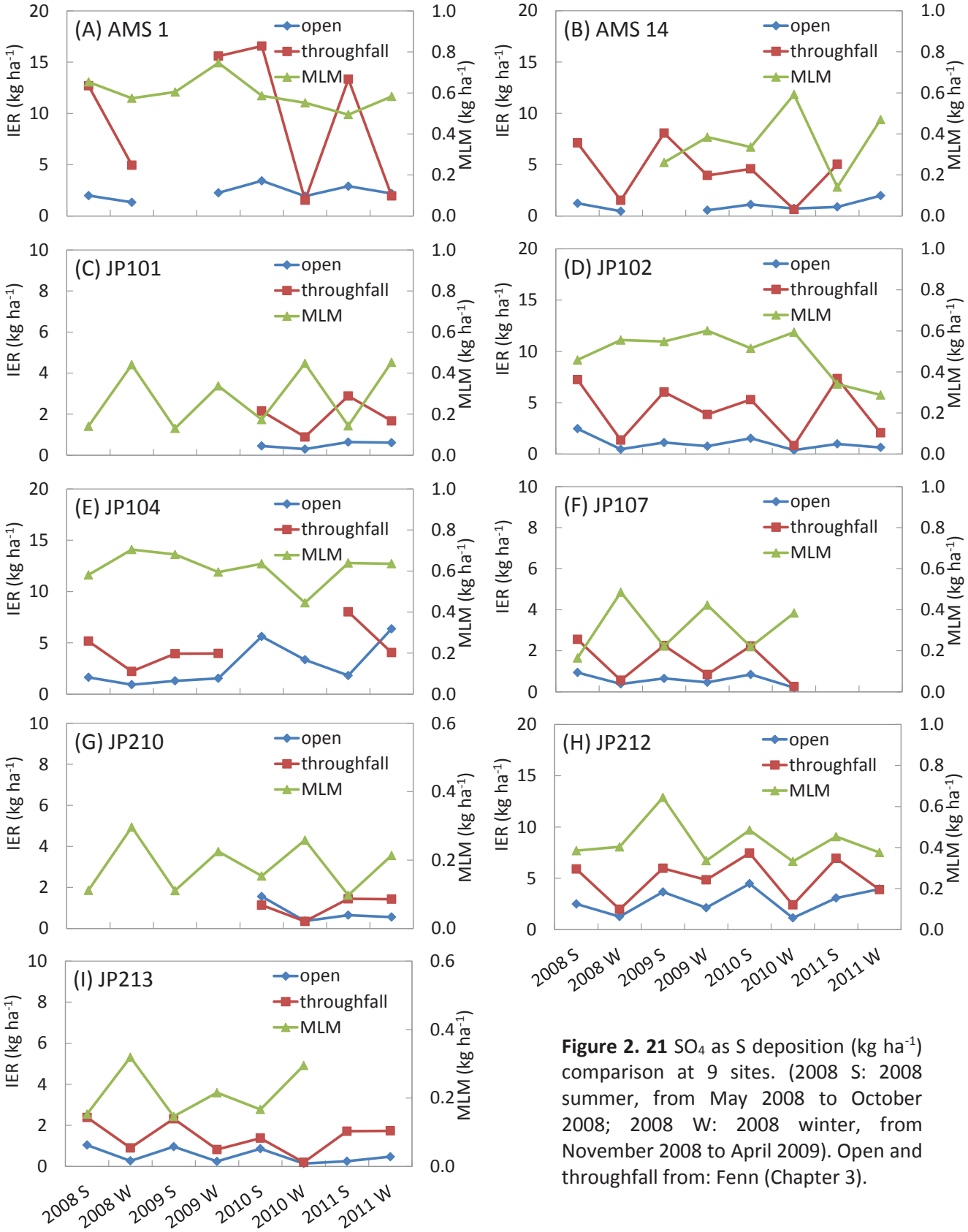

Figure 2. 21 SO_4 as S deposition (kg ha^{-1}) comparison at 9 sites. (2008 S: 2008 summer, from May 2008 to October 2008; 2008 W: 2008 winter, from November 2008 to April 2009). Open and throughfall from: Fenn (Chapter 3).

2.4 Conclusion

NO and SO_2 are the primary pollutants produced by oil sands facilities. The major emission sources are the upgrader stacks for SO_2 and stacks, mine fleets and off-, on-road vehicles for NO_x. After emitting from the sources, NO_2 and SO_2 undergo dilution and chemical reaction. As shown in figure 2.6, figure 2.11, figure 2.18 (left), and figure 2.20, both enhanced concentration and deposition were limited within a certain range (~30 km) from the emission sources. The highest NO_2 and SO_2 deposition occurred in major industrial operation areas and Fort McMurray. However, concentrations of NH_3 and HNO_3 were also greater outside of the AOSR industrial activities, mainly in its southern part. Ammonia increased levels were possibly also caused by forest fires and agricultural activities in central Alberta. Nitric acid, as the secondary pollutant produced via photochemical reactions, was found at distances from the main NO_x emission sources both in the northern and southern directions. Consequently, deposition of these pollutants as well as deposition of total gaseous inorganic N was also greater in those areas.

The comparison of the N and S deposition results calculated with the MLM with the CALPUFF modeled values (Chapter 4) found similar patterns for dry deposition estimates. The major difference between the two approaches was the total S (wet and dry) from CALPUFF (Fig. 4.2) was significantly higher than the SO_2 deposition (dry) calculated with the MLM especially near emission sources. The MLM might underestimate the SO_2 dry deposition due to its default setting. The comparison for total N deposition shows a good agreement (and a good spatial trending) between the two methods for 17 sampling sites (Appendix 2.4) except AH7, JP102, JP104 and JP212. These four sites are very close to emission sources where the CALPUFF model might overestimate the total N deposition.

The NH_4^+ deposition calculated from the passive sampler data with the MLM and determined with the IER open/throughfall sampling (Chapter 3) had similar patterns at 9 sampling sites. The NO_3^- deposition results from two methods were similar. However, SO_2 dry deposition calculated with the MLM was much lower than that from the IER sampling. Clearly a further study should be carried out for better SO_2 dry deposition estimation.

2.5 References

Ainsworth, E. E., Yendrek, C. R., Sitch, S., Collins, W. J., Emberson, L. D. 2012. The effects of tropospheric ozone on net primary productivity and implications for climate change. Annu. Rev. Plant Biol., 63, 637-661.

Brook, J.R., Zhang, L.M., Li, Y.F., Johnson, D., 1999. Description and Evaluation of a Model of Deposition Velocities for Routine Estimates of Dry Deposition over North America. Part II: Review of Past Measurements and Model Results. Atmos Environ 33, 5053-5070.

Bytnerowicz, A., Dueck, T., Godzik, S. 1998. Nitric oxide, nitrogen dioxide, nitric acid vapor and ammonia. In: R. Flagler (ed.) Recognition of Air Pollution Injury to Vegetation: a Pictorial Atlas, Air & Waste Management Association, Pittsburgh, PA, 5-1 through 5-17.

Bytnerowicz, A., Sanz, M. J., Arbaugh, M. J., Padgett, P. E., Jones, D. P., Davila A. 2005. Passive sampler for monitoring ambient nitric acid (HNO_3) and nitrous acid (HNO_2) concentrations. Atmospheric Environment, 39, 2655-2660.

Bytnerowicz, A., Schilling, S., Alexander, D., Fraczek, W., Hansen, M. 2010. Passive monitoring to estimate N (NO_2, HNO_3, NH_3) exposure in remote areas and geospatial analysis to optimize monitoring networks in the Athabasca Oil Sands Region, 103 Annual Conference and Exhibition of the Air & Waste Management Association, Calgary Canada, June 22-25, 2010, Extended Abstract 2010-A-563-AWMA.

Bytnerowicz, A., Fenn, M., Allen, E., Cisneros, R. 2014. Ecologically relevant air chemistry. In: Ecosystems of California: a Source Book, H. Mooney and E. Zavaleta, Editors, University of California Press (in print).

Clarke, J.F., Edgerton, E.S., Martin, B.E., 1997. Dry Deposition Calculations for the Clean Air Status and Trends Network. Atmos Environ 31, 3667-3678.

Cooter, E.J., Schwede, D.B., 2000. Sensitivity of the National Oceanic and Atmospheric Administration Multilayer Model to Instrument Error and Parameterization Uncertainty. J Geophys Res-Atmos 105, 6695-6707.

Finlayson-Pitts, B. J., Pitts, J. N. Jr. 2000. Chemistry of the Upper and Lower Atmosphere. Academic Press, San Diego, USA.

Hanson, P. J., and S. E. Lindberg. 1991. Dry deposition of reactive nitrogen compounds: a review of leaf, canopy and non-foliar measurements. Atmospheric Environment, 25A, 1615-1634.

Hsu, Y.-M., 2013. Trends in Passively-Measured Ozone, Nitrogen Dioxide and Sulfur Dioxide Concentrations in the Athabasca Oil Sands Region of Alberta, Canada. Aerosol and Air Quality Research. pp 1-16.

Johnstone, K., Ver Hoef, J., Krivoruchko, K., Lucas, n. 2001. Using ArcGIS Geostatistical Analyst. ESRI, Redlands, California.

Koutrakis, P., Sioutas, C., Ferguson, S. T., Wolfson, J. M., Mulik, J. D., and Burton, R. M. 1993. Development and evaluation of a glass honeycomb denuder/filter pack system to collect atmospheric gases and particles. Environmental Science & Technology, 27, 2497-2501.

Krupa, S.V., 2003. Effects of Atmospheric Ammonia (NH_3) on Terrestrial Vegetation: A Review. Environ Pollut 124, 179-221.

Krupa, S. V., and Legge, A. H. 2000. Passive sampling of ambient, gaseous air pollutants: an assessment from an ecological perspective. Environmental Pollution. 107, 31-45.

Legge, A. H., Jäger, H.–J., Krupa, S. V. 1998. Sulfur dioxide. In: R. B. Flagler (ed.) Recognition of Air Pollution Injury to Vegetation – a Pictorial Atlas. Air & Waste Management Association, Pittsburg, PA, 3-1 through 3-42.

Lovett, G. M. 1994. Atmospheric deposition of nutrients and pollutants in North America: an ecological perspective. Ecological Applications, 4, 629-650.

Magnani, F., Mencuccini, M., Borghetti, M., *et al.* (2007). The human footprint in the carbon cycle of temperate and boreal forests. *Nature*. 447: 848-450.

Meyers, T.P., Finkelstein, P., Clarke, J., Ellestad, T.G., Sims, P.F., 1998. A Multilayer Model for Inferring Dry Deposition Using Standard Meteorological Measurements. J Geophys Res-Atmos 103, 22645-22661.

Roadman, M. J., Scudlark, J. R., Meisinger, J. J., Ullman, W. J. 2003. Validation of Ogawa passive samplers for the determination of gaseous ammonia concentrations in agricultural settings. Atmospheric Environment, 37, 2317-2325.

Schwede, D., Zhang, L.M., Vet, R., Lear, G., 2011. An Intercomparison of the Deposition Models Used in the Castnet and Capmon Networks. Atmos Environ 45, 1337-1346.

Seinfeld, J.H., Pandis, S.N., 2006. Atmospheric Chemistry and Physics: From Air Pollution to Climate Change, 2nd ed. Wiley, Hoboken, N.J.

Sickles, J., Shadwick, D.S., 2007a. Changes in Air Quality and Atmospheric Deposition in the Eastern United States: 1990-2004. J Geophys Res-Atmos 112.

Sickles, J.E., Shadwick, D.S., 2007b. Seasonal and Regional Air Quality and Atmospheric Deposition in the Eastern United States. J Geophys Res-Atmos 112.

Tang, H., Lau, T., Brassard, B., Cool, W., 1999. A New All-Season Passive Sampling System for Monitoring No2 in Air. Field Anal Chem Tech 3, 338-345.

Tang, H.M., Brassard, B., Brassard, R., Peake, E., 1997. A New Passive Sampling System for Monitoring SO_2 in the Atmosphere. Field Anal Chem Tech 1, 307-314.

Tang, H.M., Lau, T., 2000. A New All Season Passive Sampling System for Monitoring Ozone in Air. Environ Monit Assess 65, 129-137.

US EPA 1998. Emission Facts: Idling Vehicle Emissions. U.S. Environmental Protection Agency Washington, DC.

Wesely, M.L., Hicks, B.B., 2000. A Review of the Current Status of Knowledge on Dry Deposition. Atmos Environ 34, 2261-2282.

Zhang, L., Vet, R., O'Brien, J.M., Mihele, C., Liang, Z., Wiebe, A., 2009. Dry Deposition of Individual Nitrogen Species at Eight Canadian Rural Sites. J Geophys Res-Atmos 114. DOI: 10.1029/2008JD010640., D02301 (13 pp).